

Panoramic Out-of-Distribution Segmentation

Mengfei Duan, Kailun Yang, Yuheng Zhang, Yihong Cao, Fei Teng, Kai Luo,
Jiaming Zhang, Zhiyong Li, and Shutao Li, *Fellow, IEEE*

Abstract—Panoramic imaging enables capturing 360° images with an ultra-wide Field-of-View (FoV) for dense omnidirectional perception. However, current panoramic semantic segmentation methods fail to identify outliers, and pinhole Out-of-distribution Segmentation (OoS) models perform unsatisfactorily in the panoramic domain due to background clutter and pixel distortions. To address these issues, we introduce a new task, Panoramic Out-of-distribution Segmentation (PanOoS), achieving OoS for panoramas. Furthermore, we propose the first solution, POS, which adapts to the characteristics of panoramic images through text-guided prompt distribution learning. Specifically, POS integrates a disentanglement strategy designed to materialize the cross-domain generalization capability of CLIP. The proposed Prompt-based Restoration Attention (PRA) optimizes semantic decoding by prompt guidance and self-adaptive correction, while Bilevel Prompt Distribution Learning (BPDL) refines the manifold of per-pixel mask embeddings via semantic prototype supervision. Besides, to compensate for the scarcity of PanOoS datasets, we establish two benchmarks: DenseOoS, which features diverse outliers in complex environments, and QuadOoS, captured by a quadruped robot with a panoramic annular lens system. Extensive experiments demonstrate superior performance of POS, with AuPRC improving by 34.25% and FPR₉₅ decreasing by 21.42% on DenseOoS, outperforming state-of-the-art pinhole-OoS methods. Moreover, POS achieves leading closed-set segmentation capabilities. Code and datasets will be available at <https://github.com/MengfeiD/PanOoS>.

Index Terms—Scene Segmentation, Panoramic Images, Out-of-Distribution Segmentation, Scene Understanding.

1 INTRODUCTION

PANORAMIC imaging technology, capable of capturing high-quality 360° images using optical systems, has gained significant attention across various omnidirectional vision tasks, such as dense visual prediction [1], [2], [3], holistic scene understanding [4], [5], [6], panoramic scene segmentation [7], [8], [9], and occlusion-aware seamless perception [10]. Especially, for embodied agents, such as autonomous vehicles and mobile robots, an omnidirectional perception facilitates a comprehensive understanding of the surroundings [11], [12], [13]. However, existing panoramic scene segmentation models are trained to recognize a predefined set of semantic classes (*e.g.*, *road*, *building*, *car*, *pedestrian*) [14], [15], [16], [17], fail to identify outliers. Due to the broader Field of View (FoV) of panoramic images and the nature of long-tail semantic distribution in unconstrained surroundings, objects that do not belong to the predefined classes (*e.g.*, *animals*, *furniture*) frequently appear in real-world driving environments, which greatly exacerbates the problem. Therefore, there is an urgent need for a technology capable of identifying outliers not present during training to avoid potential dangers.

To address the challenge and enhance comprehensive and safe omnidirectional scene understanding, we introduce a new task, termed the *Panoramic Out-of-Distribution Segmentation (PanOoS)*. Compared with pinhole out-of-distribution segmentation (pinhole-OoS), *PanOoS* offers a broader FoV beyond the pinhole view, for example, ranging from 95° to 360° as depicted in Fig. 1, enabling the detection of outliers and even dangers that are not visible from a pinhole perspective, *e.g.*, the *tiger*. Yet, panoramic images pose unique challenges in visual understanding



Fig. 1: *Panoramic Out-of-distribution Segmentation (PanOoS)* enhances comprehensive and safe omnidirectional scene perception by using a broader Field-of-View (FoV). ①: pinhole image with narrow FoV; ②: 360° panoramic image; ③: segmentation result. The *tiger* in the image is an outlier on the street.

tasks due to their broader FoV and complex scene content, which introduce pixel distortions [18], [19] and background clutter, complicating semantic interpretation. These characteristics of the panoramic image lead to feature distribution shifts and loss of semantic information, which impair the model’s ability to capture low-level features and fine details of the image. Moreover, these issues interfere with foreground object recognition, introduces semantic ambiguity in overlapping or visually similar regions, and complicates the distinction between in-distribution and out-of-distribution areas.

Although there are some effective techniques for panoramic semantic segmentation [8], [11], [20], they are designed for closed-set segmentation and do not include outlier detection. The inability to handle outliers means that these techniques may

- M. Duan, K. Yang, Y. Zhang, Y. Cao, F. Teng, K. Luo, Z. Li, and S. Li are with Hunan University, China.
- J. Zhang is with Karlsruhe Institute of Technology, Germany.
- J. Zhang is also with ETH Zürich, Switzerland.
- Corresponding authors: Kailun Yang and Zhiyong Li (e-mail: first-name.lastname@hnu.edu.cn).

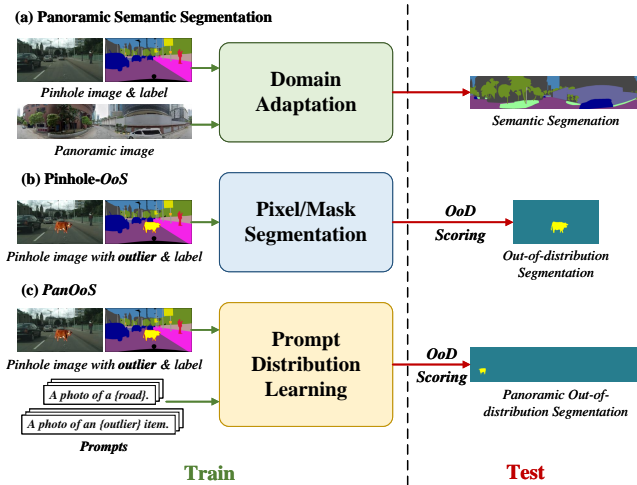


Fig. 2: **Comparison of panoramic semantic and out-of-distribution segmentation paradigms.** (a) Panoramic semantic segmentation methods adapt models from pinhole to panoramic through domain adaptation, yet remain limited to in-distribution dense predictions; (b) Pinhole-*OoS* methods combine semantic segmentation with out-of-distribution (OoD) scoring to detect outliers, but are restricted to narrow pinhole FoV; (c) POS achieves unified semantic and OoD segmentation on panoramic images via prompt distribution learning.

miss critical objects, leading to incorrect or incomplete scene understanding. This issue significantly limits their practical applicability, particularly in dynamic and unpredictable environments where outliers are frequent. High costs associated with data annotation have also resulted in a scarcity of datasets specifically designed for training panoramic segmentation. As illustrated in Fig. 2, most panoramic segmentation methods typically rely on techniques such as unsupervised domain adaptation [9], [10], [11] or knowledge adaptation [12], [21], [22] to transfer models from the pinhole to the panoramic domain. However, these approaches are not suitable for *PanOoS*, where the model must not only adapt to the characteristics of the panoramic domain, but also learn to distinguish between in-distribution regions and outliers while ensuring closed-set segmentation performance. Meanwhile, state-of-the-art *OoS* methods [23], [24], [25] for pinhole images typically involve first training a mask-based segmentation model, *e.g.*, in Mask2Former style [26], and then computing anomaly scores using various outlier detection techniques during fine-tuning or inference. Nevertheless, existing research works primarily focus on narrow-FoV pinhole images, making them ill-equipped to address the aforementioned challenges introduced by broader-FoV in panoramic images (see Fig. 3). Unlike panoramic semantic segmentation and pinhole-*OoS* tasks, *PanOoS* uniquely faces a conflict between semantic segmentation and out-of-distribution detection within the mask segmentation model architecture.

To tackle the *OoS* challenge within the panoramic domain, we propose POS, a novel mask-based framework that integrates prompt distribution learning to enhance pixel-level generalization across complex and distorted panoramic visual domains. (1) Compared to purely visual models, vision-language models are typically exposed to a broader array of visual concepts during pre-training [27]. To enhance the pixel-level perception of outliers within panoramic scenes, POS incorporates CLIP [28] into a mask-transformer architecture, leveraging its strong generalization

capabilities to better capture scene semantics. Moreover, during outlier exposure fine-tuning, POS explicitly disentangles per-pixel mask decoding from semantic classification, thereby mitigating semantic entanglement and preserving accurate mask representations for subsequent pixel-level decoding. (2) Traditional image-based query decoding methods [23], [24], [25], [26] often struggle to accurately capture semantic information under pixel distortions and background clutter. To address this limitation, we propose a Prompt-based Restoration Attention (PRA), which integrates the text encoder to extract both class-level and distributional prompts semantic information. By adaptively guiding the learning process, the PRA mechanism optimizes semantic extraction, significantly enhancing the accuracy and robustness of semantic understanding, thereby effectively mitigating semantic ambiguity in challenging panoramic scenes. (3) Finally, an innovative Bilevel Prompt Distribution Learning (BPDFL) mechanism is proposed. By leveraging the language-image semantic distribution consistency of the CLIP model, BPDFL refines the spatial distribution of per-pixel mask feature representations, strengthens the distinguishability of out-of-distribution features, and the adaptability of the pinhole-trained model to severe distortions encountered in panoramic images. With these crucial designs, POS achieves superior alignment with the characteristics of panoramic images, enabling efficient out-of-distribution segmentation while demonstrating impressive closed-set segmentation performance.

To facilitate the evaluation of the *PanOoS* task, we create two fresh datasets: (1) We have spent a large effort on artificial screening and built the first panoramic out-of-distribution segmentation dataset: Dense Panoramic Out-of-distribution Segmentation (DenseOoS), for model evaluation. Due to the broader FoV, the backgrounds of each panoramic image are very complex, featuring object instances that vary in shape and appearance, along with significant distortions. Meanwhile, outliers are randomly distributed across reasonable areas. (2) To further verify the performance of POS in practical application and explore the *PanOoS* in unconstrained, unstructured, and intense-motion real-world scenarios, we employ a quadruped mobile robot to collect the real motion scene panoramic images with outliers, creating the Quadruped Panoramic Out-of-distribution Segmentation (QuadOoS) dataset. Compared to DenseOoS, QuadOoS contains a greater number of abnormal objects in each image, with smaller sizes, while maintaining the same panoramic pixel characteristics. Ultimately, based on DenseOoS and QuadOoS, we established the evaluation benchmarks for the *PanOoS* task. The proposed POS achieves state-of-the-art performance on both two benchmarks, significantly outperforming other pinhole-*OoS* methods [23], [24], [25], [29], [30], with AuPRC, and FPR_{95} of (85.56%, 48.13%), and (0.45%, 85.22%), respectively. Furthermore, compared to panoramic semantic segmentation methods [8], [31], [32], it demonstrates superior closed-set segmentation performance, with an mIoU of 63.30%. These results collectively validate the effectiveness of the proposed POS in addressing *PanOoS* and enhancing panoramic scene understanding.

At a glance, this work delivers the following contributions:

- (1) We introduce the Panoramic Out-of-Distribution Segmentation (*PanOoS*) task, which, for the first time, explores out-of-distribution segmentation in the panoramic domain, aiming to facilitate comprehensive and holistic scene understanding.
- (2) To achieve the *PanOoS* task, we propose *POS*, a mask-transformer-based model with Prompt-based Restoration Attention (PRA) and Bilevel Prompt Distribution Learning

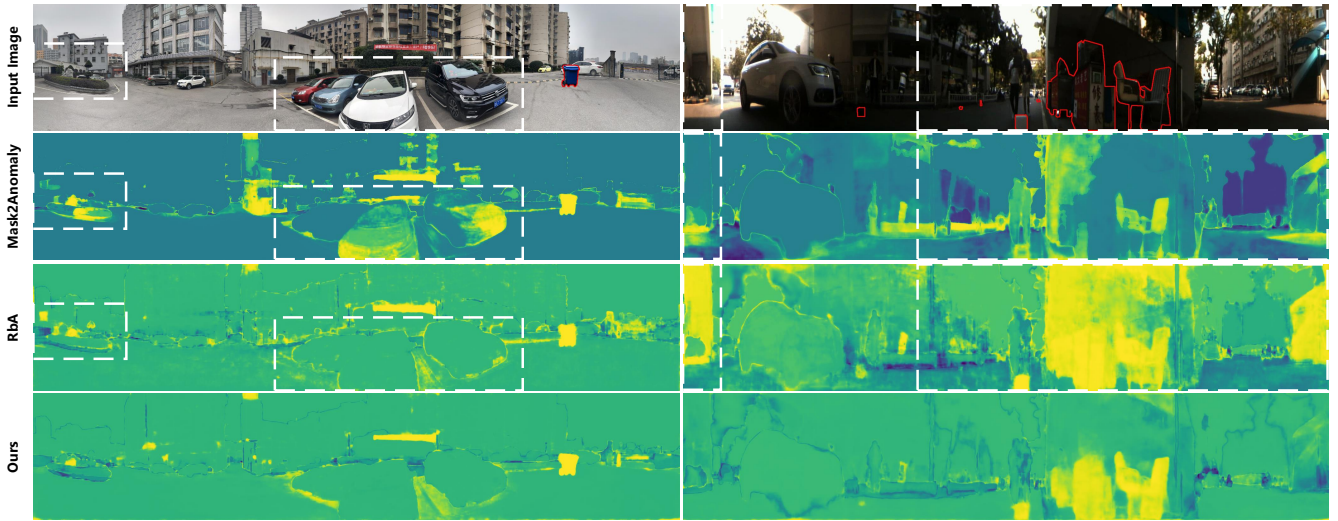


Fig. 3: **Impact of background clutter and pixel distortions** on state-of-the-art pinhole-*OoS* methods. Existing pinhole-*OoS* methods, e.g. Mask2Anomaly and RbA, fail in adapting to the background clutter and pixel distortion, resulting in a higher number of false positives. In contrast, the proposed POS effectively enhances the perception of panoramic pixels.

(BPDL), which effectively alleviates the effects of background clutter and pixel distortions, demonstrating remarkable performance.

- (3) Two fresh datasets, DenseOoS and QuadOoS, are created, serving as important benchmarks for *PanOoS* and contributing to the advancement of panoramic understanding.

2 RELATED WORK

Panoramic Semantic Segmentation. By capturing broader-FoV scenes, panoramic images serve as a starting point for a more holistic understanding of 360° surroundings [7], [33]. The first line of research on panoramic semantic segmentation [20], [34], [35], [36], [37] is based on supervised learning. However, to address the scarcity of annotations, researchers have revisited panoramic segmentation from the perspective of unsupervised domain adaptation [38], [39], [40], [41], [42] by leveraging rich training sources from narrow-FoV pinhole data. The approaches can be divided into three types: pseudo-labeling [4], [43], adversarial training [9], [17], [44], and prototype adaptation [10], [32], [45], [46], [47] methods. Pseudo-labeling generates self-supervised labels for the panoramic domain. Adversarial training enforces the target model to capture domain-invariant characteristics across domains using a discriminator. Prototype adaptation approaches align high-level feature centers between the pinhole and panoramic domains. Additionally, related work demonstrates strong performance from the perspective of knowledge adaptation [12], [21], [22]. However, existing methods focus on closed-set segmentation and do not address the problem of identifying outliers within the scene. Recently, open panoramic segmentation [6] has been proposed, but the focus has been on improving the efficiency of panoramic open-vocabulary segmentation. Different from previous works, we aim to explore out-of-distribution segmentation in panoramic images and exploit the distribution learning of semantic text-based prompts to advance panoramic scene understanding.

Out-of-distribution Segmentation. Out-of-distribution segmentation aims to identify and separate outliers in some specific scenes, such as complex driving environments [14], [48], [49],

[50], while maintaining closed-set segmentation capability. Early uncertainty-based methods assume that outliers lead to low-confidence predictions, focusing on estimating the prediction uncertainty through various ways to measure pixel-wise anomaly scores [51], [52], [53], [54], [55]. However, models trained on closed sets may make high-confidence erroneous predictions for unseen categories. Follow-up works have shifted their focus to reconstruction. Reconstruction-based methods detect outliers by comparing the differences between the original image and the reconstruction generated from semantic segmentation predictions [49], [56], [57], [58], [59], [60]. However, nearly all reconstruction-based methods are heavily dependent on the quality of the generated output, which can lead to performance degradation due to image artifacts [61]. These methods also suffer from context dependence and high computational costs, resulting in unsatisfactory performance in complex environments.

Recent approaches [29], [30], [62], [63], [64] introduce the Outlier Exposure (OE) strategy [65] that utilizes auxiliary out-of-distribution data to regularize the model’s feature space. These auxiliary outliers typically are images from other datasets (such as ImageNet [66], COCO [67], ADE20K [68], etc.) or involve cutting out abnormal objects from other images and pasting them into inlier scenes. Outliers are used for uncertainty estimation of outlier samples or fine-tuning model parameters. Notably, PEBAL [29] learns energy-based adaptive penalties through abstention learning, whereas DenseHybrid [30] combines likelihood and posterior evaluation to achieve better results. Compared to earlier works, the OE strategy yields better performance, but pixel-wise architecture methods score each pixel individually without considering local semantics, leading to increased noise in anomaly predictions. Currently, mask-transformer-based methods [23], [24], [25], [69], [70], [71] overcome this limitation by segmenting outliers into semantically clustered masks and encouraging the objectness of predictions, which achieve leading segmentation results. EAM [23] ensembles region-based outlier scores, while Mask2Anomaly [25] combines contrastive learning and mask refinement to significantly reduce false positives. RbA [24] utilizes mask queries that act

as a one-vs-all classifier [23], [24], [72], helping to eliminate uncertainty in ambiguous in-point regions, *e.g.*, semantic boundaries, by reducing the scores in negative pixels. However, existing methods primarily focus on narrow FoV pinhole images, and when transferred to the panoramic domain, they struggle to adapt to challenges such as background clutter and pixel distortions caused by the broad FoV. To the best of our knowledge, this is the first work to tackle this pressing problem in panoramic out-of-distribution segmentation.

3 METHODOLOGY

In our work, to promote a more comprehensive omnidirectional perception and leverage the advantages of panoramic broader-FoV, a novel panoramic perception task, *PanOoS*, is introduced. In response to the challenges posed by complex backgrounds and pixel distortions, we analyze the model architecture and fine-tuning strategies, ultimately proposing the first mask-based out-of-distribution segmentation model specifically designed for the established *PanOoS* task.

3.1 Problem Setting

Out-of-distribution segmentation and anomaly segmentation are inherently similar; however, more specifically, out-of-distribution segmentation encompasses anomaly segmentation. The primary distinction lies in whether the methods can segment each in-distribution category while also identifying outliers. Out-of-distribution segmentation can be achieved in per-pixel semantic segmentation architectures [23], [24], [25], [26], [70] by computing anomaly probability on top of the per-pixel classifier. For the pixel-level class scores $S(x) \in \mathbb{R}^{K \times H \times W}$ obtained by segmenting the input image $x \in \mathbb{R}^{3 \times H \times W}$ using a pixel-wise segmentation architecture, the anomaly scores $A(x) \in \mathbb{R}^{H \times W}$ are computed as follows:

$$A(x) = f(S(x)), \quad (1)$$

where K denotes the number of classes for semantic segmentation, H and W correspond to the height and width of the image, respectively.

3.2 Framework

In contrast to pinhole-*OoS*, the complex backgrounds and pixel distortions in panoramic images hinder the generalization performance of pure visual models pre-trained on pinhole image datasets. This domain adaptation barrier prevents the model from effectively learning the visual features of panoramic images, resulting in suboptimal detection performance. It is important to explore methods for transferring models trained in the pinhole domain to the panoramic domain. Despite the strong performance of the mask-transformer model [26] in pinhole-*OoS*, the current advanced masked pinhole-*OoS* methods do not translate effectively to *PanOoS*. Moreover, accurate pixel decoding is essential for panoramic segmentation. During the critical outlier exposure fine-tuning, a conflict arises between the query embedding, which favors semantic classification, and the pixel decoding, which focuses on image details. Therefore, we optimize the architecture and fine-tuning procedures, introducing POS, the first mask-transformer-based segmentation model for *PanOoS*, as illustrated in Fig. 4. The main components of the model include four parts: the image encoder, the text encoder, the pixel decoder, and the Transformer decoder.

Image Encoder. We utilize the image encoder from CLIP [28] for extracting image features and freeze its weights. The image encoder is configured as a ConvNext-Large [73] model, comprising four stages. It accepts an RGB image $x \in \mathbb{R}^{3 \times H \times W}$ as input and outputs feature maps at several resolutions to the pixel decoder. Specifically, the output feature maps are downsampled with strides of $4(c_4)$, $8(c_8)$, $16(c_{16})$, and $32(c_{32})$ relative to the input image.

Text Encoder. For the textual features, the semantic labels with K classes and the distribution labels: *inlier* and *outlier*, are integrated into the pre-designed prompt templates, *e.g.* “a photo of a {class.}”, and “a photo of an {outlier} item in the urban or rural scenes”, to obtain the text descriptions about classes and distributions. The text encoder is structured as a 16-layer transformer, each layer being 768 units wide and featuring 12 attention heads. The text descriptions are fed into text encoder to generate the prompt embeddings $\{T_i | i=0, \dots, K\} \cup \{P_{in}, P_{out}\} \in \mathbb{R}^{(K+3) \times 768}$, while T_0 represents the learnable void embedding. Further, a linear projection is used to project the prompt embeddings into the pixel space to match the dimension of the mask feature. See the Appendix A.1 for more details on prompt templates.

Pixel Decoder. Following Mask2Former [26], the pixel decoder mainly consists of 6 layers of Deformable Attention Transformer (DeformAttn) [74] and a Feature Pyramid Network (FPN) [75]. To facilitate out-of-distribution detection, the enriched semantic feature map with a stride of $32(c_{32})$ is processed with DeformAttn layers to produce f_4 , which is then passed to the Transformer decoder. Then, pixel decoder gradually unsamples and fuses feature maps (f_4 , c_{16} , c_8 , and c_4) to generate per-pixel mask embeddings $F_m(x) \in \mathbb{R}^{C_m \times H \times W}$, where C_m is the embedding dimension.

Transformer Decoder. The learnable query features $Q \in \mathbb{R}^{N \times C_q}$ are fed into the Transformer decoder layers, where they are jointly processed with the feature map f_4 and the prompt embeddings. N represents the number of object queries and C_q denotes the embedding dimension. Each decoder layer consists of a Prompt-based Restoration Attention followed by Self-attention, and a Feed-forward Network (FFN). Learnable positional embeddings are added to the query features.

Mask and region class prediction. After refining the object queries and mask feature, the refined object queries are processed through a 3-layer MLP to obtain Q for predicting N regions. Then, the membership score for each pixel belonging to a region is derived by multiplying Q with the per-pixel mask feature $F_m(x)$ and applying a *sigmoid* function:

$$M(x) = \sigma(QF_m(x)). \quad (2)$$

In parallel, the refined object queries are fed into a linear layer followed by a *softmax* function to produce posterior class probabilities $P(x) \in \mathbb{R}^{N \times K}$ for K classes:

$$P(x) = \text{softmax}(Q). \quad (3)$$

OoD Scoring. In contrast to pixel-wise semantic segmentation, the ground truth masks are divided into multiple binary masks, each containing all pixels belonging to a specific class. Ultimately, the class probabilities are broadcast to all pixels within the region, and the class score $S(x)$ is calculated as the product of the class probabilities and the mask predictions. Due to the unique architecture of the mask transformer [24], [26], [69], the class

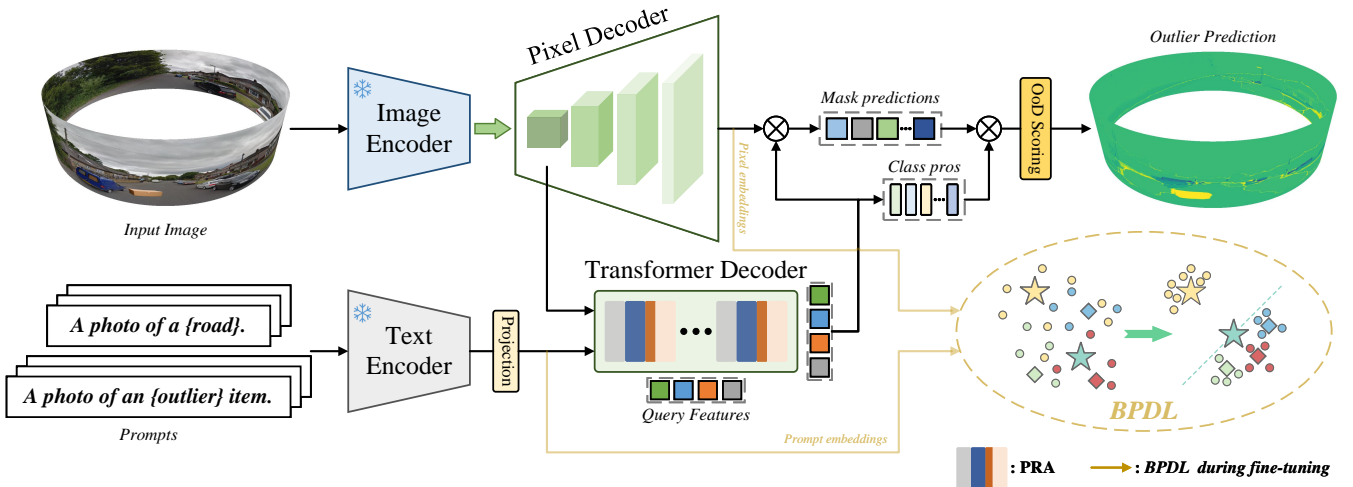


Fig. 4: **Overview of POS.** The proposed POS consists of four primary components: an image encoder, a text encoder, a pixel decoder, and a transformer decoder with Prompt-based Restoration Attention (PRA). During outlier exposure fine-tuning, Bilevel Prompt Distribution Learning (BPD L) is incorporated to optimize the pixel manifold distribution of the per-pixel mask embeddings. See Fig. 6 for details of BPD L. The image encoder extracts multi-scale panoramic image features in inference, which are then fed into the pixel decoder to generate semantically enriched features alongside the per-pixel embeddings for segmentation. Concurrently, textual prompts are embedded through the text encoder and projected into pixel space. These prompt embeddings, along with the decoded image features, are jointly processed by the transformer decoder, where they interact iteratively with learned query features. The refined queries are subsequently used for mask prediction and category classification. Finally, an out-of-distribution (OoD) scoring mechanism is applied to produce the panoramic OoD segmentation prediction.

score $S(x)$ aggregates the weighted voting scores from all object queries; after training converges, specific object queries specialize in predicting a specific class. Therefore, the outlier scoring function from *Rejected by All* [24] is adopted:

$$A(x) = RbA(S(x)) = - \sum_{k=1}^K \phi(P^T M), \quad (4)$$

with ϕ being the \tanh activation function. $A(x)$ represents the outlier score map, indicating the outliers in the image.

Panoramic-oriented Disentanglement. Existing research indicates that during fine-tuning, a balance must be maintained between mask segmentation and semantic prediction within the mask transformer [24]. *PanOoS* faces a similar conflict, and the decoding of panoramic per-pixel masks is crucial for the segmentation performance under conditions of semantic clarity. To disentangle the conflict between semantic query embedding and per-pixel mask decoding, we optimize the universal outlier exposure fine-tuning strategies, introducing a disentanglement strategy specifically designed for *PanOoS*. We observe that the performance of closed-set semantic segmentation for panoramic images during fine-tuning is crucial for identifying outliers. Specifically, the precise decoding of foreground pixels (*i.e.*, masks) determines the model’s capability to detect outliers. Thus, to fully unleash the potential of the designed model for robust segmentation, we only fine-tune the pixel decoder, mask and region class prediction of POS during the outlier exposure phase.

3.3 Prompt-based Restoration Attention

In researching semantic learning for panoramic images, we found that traditional query-based decoding is difficult to effectively capture the intricate semantic information. This limitation primarily

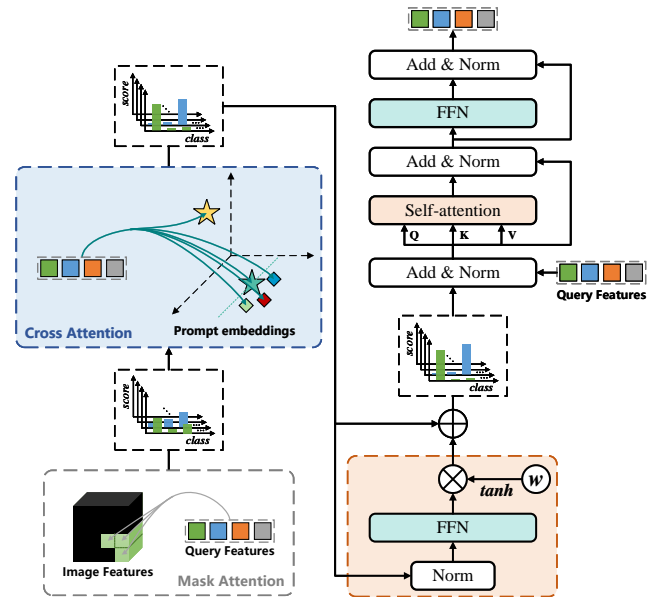


Fig. 5: **Prompt-based Restoration Attention** continuously employs masked attention and cross attention mechanisms between image features and prompt embeddings while enhancing semantic clarity through query semantic self-adaptive correction.

arises from prevalent pixel distortion and background clutter in images, which interfere with the semantic expression of queries, introduce semantic confusion, and ultimately impair the model’s comprehension of image content and segmentation performance. To address this challenge, we propose a Prompt-based Restoration Attention (PRA) module that utilizes the clear semantics embed-

ded in text prompts to guide the semantic learning of queries. A semantic self-adaptive mechanism is proposed that dynamically adjusts the learning process based on the semantic information of queries, optimizing semantic extraction and generalization.

As shown in Fig. 5, we optimize the semantic learning process for queries. Specifically, we introduce an additional Cross Attention mechanism between the class and distribution prompt embeddings and the queries, built upon the existing Masked Attention. These prompt embeddings, with their clear semantic representation, provide robust semantic guidance for the query process. By incorporating the semantic information from the prompt embeddings, we mitigate potential semantic biases in the queries during the learning process, thereby significantly enhancing the semantic accuracy of queries. The interaction between the queries, image features, and prompt embeddings is formally expressed as:

$$\hat{X}_{i,l} = \text{softmax}(\mathcal{M}_{l-1} + Q_{l-1} K_{i,l}^T) V_{i,l}, \quad (5)$$

$$\hat{X}_l = \text{softmax}(Q_l K_t^T) V_t, \quad (6)$$

where l is the layer index and $\hat{X}_l \in \mathbb{R}^{N \times C_q}$ refers to the enriched semantic queries at the l^{th} layer. $Q_{l-1}, Q_l \in \mathbb{R}^{N \times C_q}$ are obtained by linearly transforming the previous queries X_{l-1} and $\hat{X}_{i,l} \in \mathbb{R}^{N \times C_q}$ with learnable transformations, respectively. \mathcal{M}_{l-1} denotes the attention mask [26]. $K_{i,l}, V_{i,l} \in \mathbb{R}^{H_i W_i \times C_q}$ are the image features under learnable transformations respectively, and H_l, W_l are the spatial resolution of image features. $K_t, V_t \in \mathbb{R}^{(K+3) \times C_q}$ are the prompt embeddings extracted by the text encoder under learnable transformations, respectively.

To further enhance the adaptability of query semantics, we propose a semantic self-adaptive correction mechanism, which dynamically adjusts the semantic representation of the query, allowing it to better adapt to complex pixel distributions and background information in the image, formally expressed as:

$$X_l = \hat{X}_l + \text{FFN}(\text{LN}(\hat{X}_l)) \cdot \tanh(\mathcal{W}). \quad (7)$$

Here, LayerNorm (LN) is applied, and \mathcal{W} represents the learnable *adaptive weight*. We initialize the weight value to zero to ensure the adaptation to diverse multi-scale image features while retaining the training stability. Through the adaptive mechanism, the query dynamically adjusts its representation based on learned semantic information, thereby enhancing semantic generalization.

The proposed PRA fully leverages the clearer semantic information in prompt embeddings and incorporates an adaptive semantic correction mechanism. This not only optimizes the semantic learning process but also significantly enhances the accuracy and robustness of query semantic decoding, providing strong support for panoramic scene understanding.

3.4 Bilevel Prompt Distribution Learning

The pervasive pixel distortions and background clutter in panoramic images often result in a dispersed pixel manifold. This dispersion adversely affects the performance of deep neural networks, which tend to map the unknown samples inside the known class clusters instead of an arbitrary distribution in the whole feature space. Consequently, this misalignment distorts the voting scores of the pixel manifold, particularly in out-of-distribution regions within known classes, ultimately leading to overconfident and unreliable predictions. CLIP, which is trained on large-scale vision-language data pairs, demonstrates robust

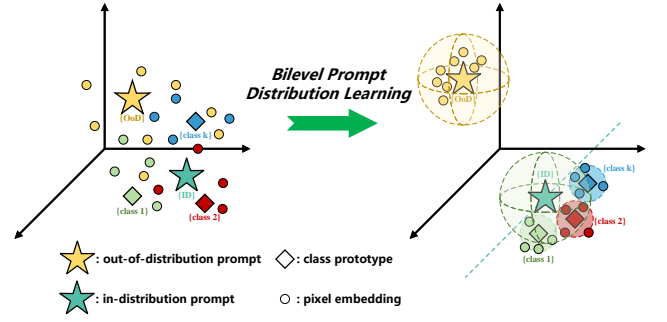


Fig. 6: The demonstration of the process of **Bilevel Prompt Distribution Learning**. The distribution prompts, text prompts for each class, and pixel embeddings are represented by stars, diamonds, and circles, respectively. The dashed circles indicate equidistant lines from the semantic center, and the dashed lines represent the decision boundary separating in- and out-of-distribution regions.

cross-domain generalization capabilities, enabling it to effectively capture the semantic information of panoramic images. Moreover, its pretrained text encoder adeptly constructs the semantic feature distribution of known classes while maintaining consistency with the pixel space distribution. This accurate semantic feature distribution provides a reliable reference for pixel manifold learning. Leveraging this foundation, we propose a Bilevel Prompt Distribution Learning (DPDL) loss, which utilizes projected class and distribution prompts $\{T_i | i=0, \dots, K\} \cup \{P_{in}, P_{out}\} \in \mathbb{R}^{(K+3) \times C_m}$, to optimize the spatial distribution of per-pixel embeddings $F_m(x)$ for mask segmentation.

As shown in Fig. 6, its core objective is to enhance the discriminability of out-of-distribution embeddings $\{O_i | i=1, \dots, N_o\} \in \mathbb{R}^{N_o \times C_m}$ at the decision boundary, thereby improving the model’s capability to accurately identify out-of-distribution regions. Specifically, the bilevel prompt distribution learning optimizes per-pixel embeddings at two levels (in- and out-of-distribution) across four key aspects.

In-distribution learning. To prevent the model from misinterpreting intra-class pixel embeddings when distinguishing out-of-distribution from in-distribution pixel embeddings $\{m_i | i=1, \dots, N_i\} \in \mathbb{R}^{N_i \times C_m}$, thereby improving closed-set segmentation performance, we introduce an in-distribution loss \mathcal{L}_{pixel} . As shown in Fig. 7, it guides the model’s learning process by enhancing intra-class pixel embedding compactness while preserving inter-class separability.

First, we minimize the Euclidean distance between each pixel embedding and the corresponding class center, optimizing intra-class compactness, which can be represented as follows:

$$\mathcal{L}_{intra} = \frac{1}{N_i} \sum_{i=1}^{N_i} \|m_i - T_{k_i}\|_2^2, \quad (8)$$

where k_i represents the class label of the in-distribution pixel embedding m_i .

As demonstrated in prior works [76], [77], increasing the inter-class distance between category centers helps mitigate semantic ambiguity across different classes. Building upon this insight, similarly, an inter-class separation loss \mathcal{L}_{inter} is proposed to refine the classification boundaries in the feature space. Unlike existing approaches that rely on learned or manually defined class

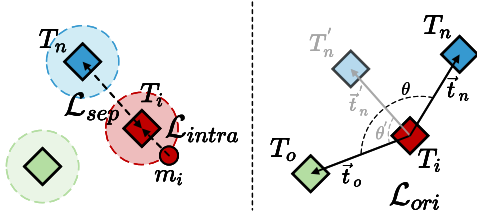


Fig. 7: **In-distribution Learning.** Enhancing intra-class compactness: the similarity of pixel embeddings within the same class is reinforced, resulting in a more compact distribution of intra-class features. Improving inter-class separation: the embedding distance between different classes is expanded, thereby strengthening the discriminability of inter-class features.

centers, our method leverages semantically clear text prompts as predefined category prototypes, which inherently exhibit better separation due to their linguistic distinctness. The proposed \mathcal{L}_{inter} then acts as a regularization term to further constrain the feature distribution, ensuring structured separation and preventing uncontrolled dispersion of embeddings. We primarily propose an separation loss \mathcal{L}_{sep} that increases the distance between each class center T_i and its nearest negative class center T_n :

$$\mathcal{L}_{sep} = \frac{1}{K+1} \sum_{i=0}^K \max(s - \min_{n \neq i} \|T_i - T_n\|_2^2, 0). \quad (9)$$

The distance margin s is defined as a hyperparameter. In addition, to account for the spatial relationships among the remaining negative class centers in the feature space, we introduce an additional orientation constraint \mathcal{L}_{ori} to optimize the directional relationships of class embedding distributions. As shown in Fig. 7 (right), when repelling the nearest negative class center T_n , the angle θ between the direction \vec{t}_n (from T_i to T_n) and the direction \vec{t}_o (from T_i to other negative class centers T_o) tends to increase:

$$\begin{aligned} \vec{t}_n &= T_n - T_i, \\ \vec{t}_o &= T_o - T_i, \end{aligned} \quad (10)$$

$$\mathcal{L}_{ori} = \frac{1}{K+1} \sum_{i=0}^K \sum_{o \neq i, n} \omega_o (1 + \cos(\vec{t}_n, \vec{t}_o)), \quad (11)$$

where ω_o represents the weights assigned to other negative class centers $T_{o \neq i, n}$, which are determined based on their spatial relationships relative to T_n :

$$\omega_o = \frac{\exp(-\|T_n - T_o\|_2)}{\sum_{k \neq i, n} \exp(-\|T_n - T_k\|_2)}. \quad (12)$$

The inter-class separation loss \mathcal{L}_{inter} is formulated as combination of two key terms:

$$\mathcal{L}_{inter} = \mathcal{L}_{sep} + \mathcal{L}_{ori}. \quad (13)$$

Ultimately, the in-distribution pixel learning loss \mathcal{L}_{pixel} is defined as a sum of the intra-class compactness loss \mathcal{L}_{intra} and inter-class separation loss \mathcal{L}_{inter} , formulated as follows:

$$\mathcal{L}_{pixel} = \mathcal{L}_{intra} + \mathcal{L}_{inter}, \quad (14)$$

The \mathcal{L}_{pixel} facilitates that, while capturing the overall feature space distribution, the model further refines its ability to differentiate in-distribution class distributions and enhances its semantic understanding.

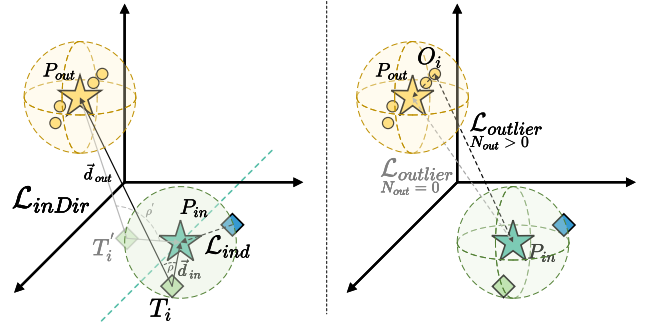


Fig. 8: **Distribution Learning.** Isolation of out-of-distribution pixels: A distinct boundary is established in the feature space to separate out-of-distribution regions from known class regions, thereby reducing the model’s overconfidence in out-of-distribution areas. Aggregation of out-of-distribution pixels: through semantic guidance, out-of-distribution pixel embeddings are clustered into specific semantic spaces, preventing their dispersion and interference with the feature distribution of known classes.

Distribution learning. Building upon in-distribution learning, we propose a higher-level distribution learning mechanism to enhance the separability of out-of-distribution embeddings O_i and achieve a more precise delineation of the overall feature space.

To establish a robust foundation for semantic alignment in subsequent distribution region partitioning and enable the model to more accurately capture the feature distribution patterns of known classes, we first minimize the distance between class text prompts $\{T_i \mid i = 0, \dots, K\}$ and in-distribution prompts P_{in} in the feature space. The in-distribution compactness loss \mathcal{L}_{ind} promotes that the feature distribution of known classes aligns with the in-distribution semantic information:

$$\mathcal{L}_{ind} = \frac{1}{K+1} \sum_{i=0}^K \|T_i - P_{in}\|_2^2. \quad (15)$$

To further constrain the distributional difference between known class features and unknown pixel features, we propose a directional constraint strategy. As depicted in Fig. 8, our goal is to position known class embeddings in the opposite direction of the out-of-distribution prompt P_{out} . Specifically, we define the direction from known class embeddings to P_{in} as \vec{d}_{in} and the direction to P_{out} as \vec{d}_{out} . We optimize these directions to be as aligned as possible by maximizing their cosine similarity. The \vec{d}_{in} and \vec{d}_{out} are formulated as:

$$\begin{aligned} \vec{d}_{in} &= P_{in} - T_i, \\ \vec{d}_{out} &= P_{out} - T_i. \end{aligned} \quad (16)$$

This approach effectively mitigates confusion between in-distribution and out-of-distribution pixel embeddings in the feature space, thereby enhancing the model’s robustness to unknown features. The in-distribution directional loss \mathcal{L}_{inDir} is defined as follows:

$$\mathcal{L}_{inDir} = \frac{1}{K+1} \sum_{i=0}^K 1 - \cos(\vec{d}_{in}, \vec{d}_{out}). \quad (17)$$

The overall in-distribution loss \mathcal{L}_{inlier} is formulated as the weighted combination of the in-distribution compactness loss \mathcal{L}_{ind} and directional loss \mathcal{L}_{inDir} :

$$\mathcal{L}_{inlier} = \alpha \mathcal{L}_{ind} + \mathcal{L}_{inDir}, \quad (18)$$

where α is the contribution weight hyperparameter of \mathcal{L}_{ind} .

Furthermore, to enhance the model’s ability to identify out-of-distribution regions, we employ semantic guidance to cluster out-of-distribution pixel embeddings $\{O_1, \dots, O_{N_o}\}$ into specific regions of the semantic space. This approach not only preserves the stability of the known class feature distribution but also provides clear semantic attribution for out-of-distribution features. Additionally, it distinctly delineates out-of-distribution regions in the feature space, establishing a clear boundary with known class regions. As a result, it reduces the model’s overconfidence in out-of-distribution areas and enhances the reliability of detection.

During the fine-tuning, outliers are pasted into the input images with a preset probability. This outlier exposure strategy simulates the appearance of out-of-distribution samples in real-world scenarios, enabling the model to better adapt to complex tasks in open environments. To facilitate model learning, we propose an out-of-distribution pixel loss $\mathcal{L}_{outlier}$ for both the presence and absence of outliers:

$$\mathcal{L}_{outlier} = \begin{cases} \frac{1}{N_o} \sum_{i=1}^{N_o} \max(D_{i,out} - D_{i,in} + d, 0), & N_o > 0 \\ \max(d - \|P_{out} - P_{in}\|_2^2, 0), & N_o = 0 \end{cases}, \quad (19)$$

where $\{D_{i,out}, D_{i,in}\} = \{\|O_i - P_{out}\|_2^2, \|O_i - P_{in}\|_2^2\}$, d quantifies the degree of difference between P_{in} and P_{out} within the semantic space. The distribution learning loss \mathcal{L}_{distri} is formulated as a sum of the in-distribution loss \mathcal{L}_{inlier} and the out-of-distribution pixel loss $\mathcal{L}_{outlier}$, which is calculated as follows:

$$\mathcal{L}_{distri} = \mathcal{L}_{inlier} + \mathcal{L}_{outlier}. \quad (20)$$

Finally, the bilevel prompt distribution learning loss is defined as follows:

$$\mathcal{L}_{bpdl} = \mathcal{L}_{pixel} + \mathcal{L}_{distri}. \quad (21)$$

Through the bilevel prompt distribution learning mechanism, the manifold of per-pixel embeddings for mask segmentation becomes more compact and distinguishable, thereby demonstrating better robustness and generalization in *PanOoS*.

3.5 Loss Settings

Following [24], [25], [26], during training, bipartite matching is employed to match each ground truth mask with an object query, supervised by region prediction and classification losses, while the fine-tuning phase further incorporates outlier supervision and bilevel prompt distribution learning. For region prediction, a weighted combination of binary cross-entropy loss and Dice loss [78]:

$$\mathcal{L}_{mask} = \lambda_{bce} \mathcal{L}_{bce} + \lambda_{dice} \mathcal{L}_{dice}, \quad (22)$$

is applied to the binary mask predictions, and cross-entropy loss \mathcal{L}_{cls} is used for classification to learn the semantic classes of each mask. The total training loss is defined as follows:

$$\mathcal{L} = \mathcal{L}_{mask} + \lambda_{cls} \mathcal{L}_{cls}. \quad (23)$$

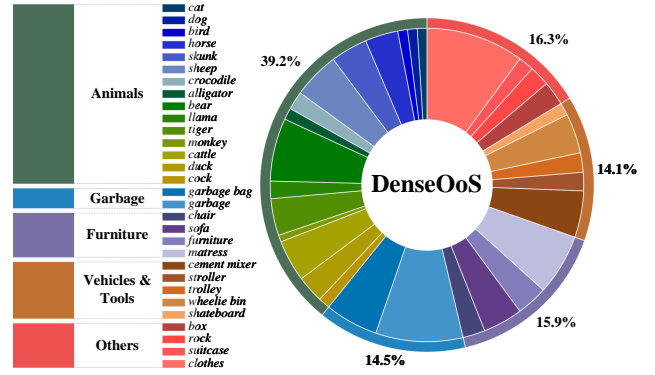


Fig. 9: **Distribution details of DenseOoS.** DenseOoS contains 30 distinct out-of-distribution classes, divided into 5 main categories: Animals, Garbage, Furniture, Vehicles & Tools, and Others.

In the outlier exposure fine-tuning phase, we further utilize the *RbA* loss \mathcal{L}_{rba} [24] to suppress the high-confidence probabilities of outlier pixels in known classes, and the bilevel prompt distribution learning loss \mathcal{L}_{bpdl} to refine the pixel manifold of per-pixel mask embeddings:

$$\mathcal{L}_{oe} = \mathcal{L} + \mathcal{L}_{rba} + \lambda_{bpdl} \mathcal{L}_{bpdl}, \quad (24)$$

where λ_{bpdl} is the balancing coefficient.

4 ESTABLISHED BENCHMARKS

4.1 Overview of the Benchmarks

In this work, we establish two novel benchmarks: DenseOoS and QuadOoS, specifically designed for *PanOoS*. 360° panoramas have a broader FoV and many small objects in the images, which exaggerate the costs of creating pixel-wise annotations in unconstrained surroundings. From the perspective of the task, we aim to overcome the scarcity of *PanOoS* testbeds and effectively evaluate the impact of mitigating the background clutter and severe distortions on out-of-distribution segmentation performance when unmasking the narrow FoV. Furthermore, to explore *PanOoS* in real-world, unconstrained, unstructured, and dense-motion scenarios, we utilize a quadruped mobile robot to capture images in outdoor motion scenes with outliers, creating a real-world benchmark. Our objective with two benchmarks is to provide a comprehensive evaluation of methods capable of performing *PanOoS*. For comparison to previous pinhole-*OoS* methods, we adapt Area under PRC Curve (AuPRC/AP), and False Positive Rate at a true positive rate of 95% (FPR₉₅) for panoramic out-of-distribution segmentation pixel-wise evaluation, mean Intersection-over-Union (mIoU) for closed-set segmentation evaluation. We unfold a comprehensive explanation in Sec 5.3.

4.2 DenseOoS

We introduce a novel test dataset: Dense Panoramic Out-of-Distribution Segmentation (DenseOoS) tailored for *PanOoS*. DenseOoS comprises a labeled test set of 1,000 panoramic images with a size of 2048×400 pixels and provides pixel-wise annotations for the *PanOoS* task, which greatly extends semantic labels from DensePASS [17]. Relevant studies have shown that using generated outlier data for model training or evaluation is an effective approach [79], [80]. Therefore, based on the

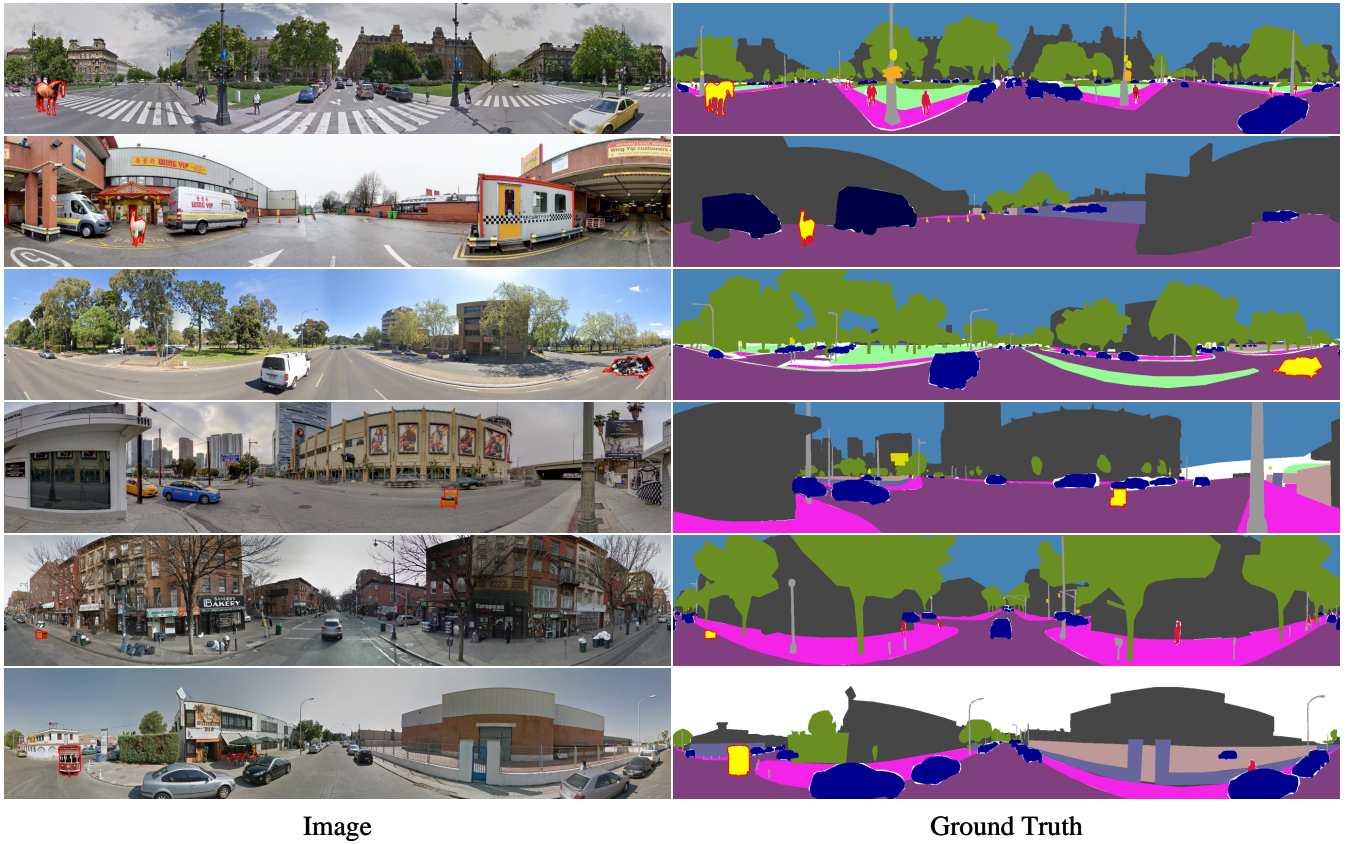


Fig. 10: **Examples from the DenseOoS dataset.** The background of the images is highly cluttered, and the distortions are significant. Outliers are distributed in reasonable areas within the image.

DensePASS dataset, we utilize a state-of-the-art image generation technique: POC [80], to place multiple classes of outliers in images while generating annotation labels for these outliers to construct DenseOoS.

The normal labels cover 19 classes that align with the Cityscapes [14], while the abnormal labels contain 30 classes of outliers as demonstrated in Fig 9, such as *animals*, *garbage*, and *furniture etc.* It additionally includes 5 other common anomalous objects (*cattle*, *duck*, *cock*, *box*, and *rock*) compared to POC [80]. To ensure the high quality and rationality of the generated images, particularly that the outliers are generated in realistic areas within the real street backgrounds, our screening process follows the “preliminary screening → independent screening → voting” workflow, eliminating unreasonable object locations, and normal situations, *e.g.*, birds flying in the city sky and garbage/garbage bags/wheelie bin placed on the side of the sidewalk.

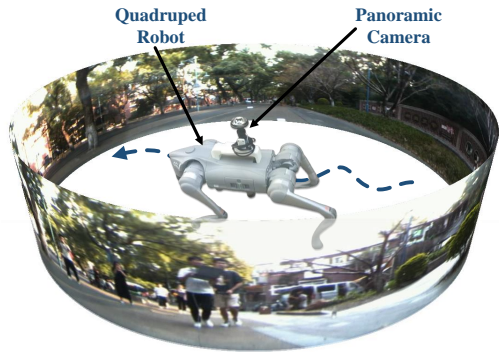
The overall process of dataset generation and construction is as follows. First, all text prompts for image inpainting (*a good photo of a {class}*) are determined based on the DensePASS validation dataset; Next, we select appropriate regions to be inserted (*e.g.*, the *road* and *sidewalk*) and the selected rectangular area is scaled to match the resolution of the real panoramic images. Then, we set different random seeds and use the POC algorithm to batch-generate images and outlier annotations. Finally, the suitable images for constructing the DenseOoS dataset are determined through preliminary manual screening, independent screening, and majority voting. Specifically, a total of 14,031 images are generated, of which 1,244 are retained after preliminary manual

screening. Following an independent screening and voting process by three examiners, we ultimately select 1,000 images for the construction of DenseOoS. As shown in Fig. 10, the outliers are diverse and distributed within reasonable areas of the images. A significant portion of these outliers extends beyond the pinhole narrow FoV, making them particularly suitable for the evaluation of the *PanOoS* task.

4.3 QuadOoS

To further explore the challenges of *PanOoS* task in real applications, we collect panoramic images featuring outliers in unconstrained, unstructured, and dense-motion real scenes, manually annotating these outliers to establish the first Quadruped Panoramic Out-of-distribution Segmentation dataset, QuadOoS. This dataset provides a crucial foundation for panoramic out-of-distribution segmentation research, facilitating the evaluation and optimization of *PanOoS* models in complex environments.

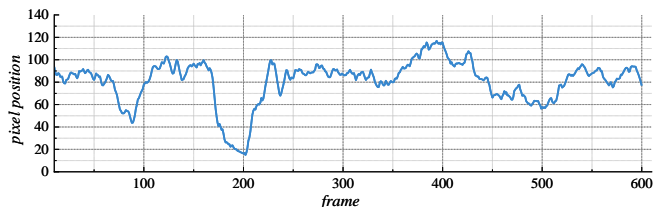
We develop a mobile platform using a quadruped robot, and the robot was selected for its biomimetic gait, a complex form of locomotion found in nature, which introduces additional challenges for *PanOoS*. The robot measures $70\text{cm} \times 31\text{cm} \times 40\text{cm}$, with a maximum payload capacity of 7kg . It can navigate vertical obstacles up to 15cm and inclines up to 30° , making it highly maneuverable in everyday environments. With 12 joint motors, the robot replicates realistic walking motions at speeds up to 2.5m/s . For sensing, we use a customized panoramic annular camera to capture a broader FoV ($360^\circ \times 70^\circ$). The camera has a pixel size of $3.45\mu\text{m} \times 3.45\mu\text{m}$, a resolution of 5 million effective



(a) Data collection platform for QuadOoS dataset.

| | Frames | Resolution | Locations | Objects | Annotations |
|------|--------|------------|-----------|---------|-------------|
| Test | 106 | 2048×400 | 8 | ≥18 | 735 |

(b) Details of the QuadOoS dataset.



(c) Y-axis pixel positions of motion trajectories.

Fig. 11: (a) Quadruped robot platform with a panoramic annular camera; (b) is the data statistics; (c) Y-axis pixel positions of quadruped robot motion trajectories. While in motion, the quadruped robot experiences significant vertical jitter.

pixels. Mounted on the quadruped robot (see Fig. 11a), the camera ensures an unobstructed, optimal field of view.

Using this platform, we conduct data collection in campus environments with outliers, creating a Quadruped Panoramic Out-of-distribution Segmentation (QuadOoS) dataset. In particular, we collect data across 8 blocks in and around the campus, with each block averaging approximately 50m in length. We pre-place the outliers and subsequently perform the actual data collection using the platform outlined in the main text. The collected images consist of a total of 4,800 frames (600 frames per block), each with an original size of 2048×476 pixels. To avoid misleading the model due to excessive exposure at the center of the lens and to maintain consistency with DenseOoS, we crop the upper portion of the original images (*i.e.*, the sky), which does not affect fair evaluation. Subsequently, to ensure the diversity of outliers and the satisfactory imaging quality, we retain a final selection of 106 original panoramic images after manual screening by five examiners, thereby constructing the QuadOoS dataset. Detailed information is provided in Fig. 11b, and see Appendix B.1 for details of the types of outliers.

Due to the gait of the quadruped robot, the collected panoramic images exhibit irregular shaking, particularly along the Y-axis (see Fig. 11c). Compared to panoramic images captured under static conditions, the images in QuadOoS present significant challenges to existing methods, such as uneven exposure, color inconsistencies due to the broader FoV, and increased motion blur, as rapid relative displacement between moving objects and the background intensifies the blurring effect. As shown in Fig. 12, each image contains an average of 7 outliers, accurately reflecting real-world situations and posing substantial challenges for *PanOoS* methods. As illustrated in Table 1, with a broader FoV (360°×70°), QuadOoS significantly differs from traditional pinhole-*OoS* datasets [48], [49], [50], [53], and complements DenseOoS by enabling the exploration of motion-induced and panoramic-specific challenges in *PanOoS*.

5 EXPERIMENT RESULTS AND ANALYSIS

5.1 Datasets

We train the model on Cityscapes [14] and extra inlier dataset: Mapillary Vistas [81] for outlier exposure fine-tuning. For *PanOoS* evaluation, we use DenseOoS and QuadOoS benchmarks. Additionally, we also use Road Anomaly [49] to evaluate pinhole-*OoS*.

| Datasets | Year | Domain | Annotation | OOD realism | No shift |
|------------------------|------|-----------|------------|-------------|----------|
| Road Anomaly [49] | 2019 | | outlier | ✓ | ✗ |
| Fishscapes L&F [50] | 2019 | | outlier | ✓ | ✓ |
| Fishscapes Static [50] | 2019 | Pinhole | outlier | ✗ | ✓ |
| StreetHazards [53] | 2019 | | all | ✓ | ✗ |
| SMIYC RA-21 [48] | 2021 | | outlier | ✓ | ✗ |
| SMIYC RO-21 [48] | 2021 | | outlier | ✓ | ✗ |
| DenseOoS | 2025 | Panoramic | all | ✓ | ✓ |
| QuadOoS | 2025 | | outlier | ✓ | ✓ |

TABLE 1: Comparison of different OoS datasets. Referring to POC [80], we qualitatively compare datasets on two main axes. We also score them as either good (✓), medium (✓) or bad (✗).

- **Cityscapes** consists of 2,975 training and 500 validation images and contains 19 categories which are considered as inliers in out-of-distribution segmentation benchmarks, such as *road*, *sky*, *building*, and *car* etc.
- **Mapillary Vistas** is a large-scale street-level image dataset containing 25,000 high-resolution images with a variety of weather, season, time of day, camera, and viewpoint, providing rich visual information.
- **Road Anomaly** is a collection of 60 web images with diverse anomaly objects on or near the road.

5.2 Implementation Details

Closed-Set Training. We follow [26] and adopt the same training recipe and losses without any special design. The difference is that we adopt the ConvNeXt-Large CLIP [73] from OpenCLIP [82], pre-trained on the LAION-2B dataset [83], and freeze its weights. In reference to previous research works [24], [25], only one decoder layer with 100 queries is used in the transformer decoder. Both dimensions C_m and C_q are set to 256. The model is trained for 90k iterations using a batch size of 16 on 4 NVIDIA GeForce RTX 3090 GPUs. The training is optimized with AdamW optimizer and weight decay 0.05. We employ the initial learning rate 1×10^{-4} and a polynomial schedule.

Outlier Exposure Fine-tuning. After the model is trained on the closed-set setting, we fine-tune the pixel decoder, 3-layer MLP, and Linear layers for 30k iterations on the inlier set of Cityscapes [14] and Mapillary Vistas [81] using the setting of the closed-set training; AdamW optimizer with 0.05 weight decay and 1×10^{-4} initial learning with polynomial schedule. For every inlier image used in fine-tuning, an object from the MS-COCO



Fig. 12: **Examples from the established QuadOoS dataset.** The images come with challenges such as uneven exposure, color inconsistencies due to the broader FoV, and increased motion blur. A large number of small outliers are scattered in the background.

samples [67] is uniformly chosen as an outlier and pasted on the image using AnomalyMix [29] with a probability p_{out} (set to 0.3), which is independent for each image.

5.3 Evaluation Metrics

In the context of the *Panoramic Out-of-distribution Segmentation (PanOoS)* benchmark, we employ three metrics, namely Area under PRC Curve (AuPRC), False Positive Rate at a true positive rate of 95% (FPR_{95}), and mean Intersection-over-Union (mIoU), to evaluate the performance of models. We provide a detailed explanation. For pixel-wise evaluation, $\mathcal{G} \in \{\mathcal{G}_{in}, \mathcal{G}_{out}\}$ is the annotated ground truth labels for an image containing outliers, where \mathcal{G}_{in} and \mathcal{G}_{out} represents the inlier and outlier labels, respectively. Let \mathcal{G}_p denote the model prediction obtained by a threshold τ . The True Positive Rate (TPR), precision, and recall can be written as:

$$TPR(\tau) = recall(\tau) = \frac{|\mathcal{G}_p \cap \mathcal{G}_{out}|}{|\mathcal{G}_{out}|}, \quad (25)$$

$$precision(\tau) = \frac{|\mathcal{G}_p \cap \mathcal{G}_{out}|}{|\mathcal{G}_p|}. \quad (26)$$

The AuPRC can be approximated as:

$$AuPRC = \int_{\tau} precision(\tau) recall(\tau). \quad (27)$$

The AuPRC works well for unbalanced datasets, which makes it particularly suitable for out-of-distribution segmentation since all the datasets are significantly skewed. Next, we consider the FPR_{95} , an important criterion for safety-critical applications, which is calculated as:

$$FPR_{95} = FPR(\tau_{95}) = \frac{|\mathcal{G}_p(\tau_{95}) \cap \mathcal{G}_{in}|}{|\mathcal{G}_{in}|}, \quad (28)$$

where τ_{95} is a threshold when TPR is 95%.

To effectively evaluate the in-distribution segmentation performance of the model, the standard mIoU is used for performance evaluation. The Intersection-over-Union (IoU) measures the overlap between predicted semantic segment p and ground truth semantic segment g , while mIoU is the mean of IoU for each class in the dataset. It is calculated as:

$$mIoU = \frac{1}{K} \sum_{k=1}^K \frac{p_k \cap g_k}{p_k \cup g_k}. \quad (29)$$

| Method | PanOoS | | | QuadOoS | | Mean | |
|-------------------|------------------|--------------------------------|-----------------|------------------|--------------------------------|------------------|--------------------------------|
| | AuPRC \uparrow | FPR ₉₅ \downarrow | mIoU \uparrow | AuPRC \uparrow | FPR ₉₅ \downarrow | AuPRC \uparrow | FPR ₉₅ \downarrow |
| PEBAL [29] | 16.39 | 7.59 | 46.29 | 11.34 | <u>39.25</u> | 13.87 | <u>23.42</u> |
| DenseHybrid [30] | 24.44 | 7.74 | 45.19 | 19.09 | 33.86 | 21.77 | 20.80 |
| EAM [23] | 17.97 | <u>6.46</u> | <u>61.58</u> | 33.05 | 79.66 | 25.51 | 43.06 |
| Mask2Anomaly [25] | 36.28 | 8.79 | 48.10 | 25.93 | 92.55 | 31.10 | 50.67 |
| RbA [24] | <u>51.31</u> | 21.87 | 57.54 | <u>34.12</u> | 90.34 | <u>42.71</u> | 56.11 |
| Ours | 85.56 | 0.45 | 63.30 | 48.13 | 85.22 | 66.85 | 42.84 |

TABLE 2: **Panoramic out-of-distribution segmentation quantitative evaluation:** POS shows significant improvement over baseline per-pixel and mask-transformer-based pinhole-*OoS* methods on *PanOoS*. Higher values for AuPRC, and mIoU are better, whereas for FPR₉₅ lower values are better. The best and second best results are **bold** and underlined, respectively, and the line in-between the table divides the per-pixel architecture and mask-transformer-based methods.

| Method | mIoU |
|----------------------|--------------|
| DAFormer [31] | 44.53 |
| Trans4PASS (T) [8] | 44.93 |
| Trans4PASS (S) [8] | 49.35 |
| Trans4PASS+ (T) [32] | 49.29 |
| Trans4PASS+ (S) [32] | 50.11 |
| 360SFUDA++ [46] | <u>50.46</u> |
| Ours | 63.30 |

TABLE 3: **Quantitative closed-set segmentation results** on DenseOoS. POS achieves outstanding panoramic semantic segmentation performance.

5.4 Results of Panoramic Out-of-distribution Segmentation

We deliver *PanOoS* results on DenseOoS and QuadOoS benchmarks. Two representative types of existing state-of-the-art pinhole-*OoS* methods, pixel-wise architecture, and mask-transformer-based methods, are benchmarked. As shown in Table 2, mask-transformer-based *OoS* methods demonstrate strong potential. Compared to the best-performing method RbA [24], POS outstrips it by large margins of 34.25% in AuPRC, 21.42% in FPR₉₅, and 5.76% in mIoU on DenseOoS. Furthermore, state-of-the-art panoramic semantic segmentation models [8], [31], [32], [46] are compared (see Table 3). Existing panoramic semantic segmentation methods cannot distinguish between in- and out-of-distribution regions and are hindered by outliers, resulting in degraded closed-set segmentation performance. However, POS achieves excellent out-of-distribution segmentation while maintaining outstanding in-distribution segmentation performance, demonstrating the strong potential of prompt distribution learning in omnidirectional scene perception. We further explore *PanOoS* in unconstrained, unstructured, and dense-motion real-world scenarios, where all baseline methods struggle to make accurate predictions under motion blur, resulting in significant false positive issues. Specifically, pixel-wise methods are not very sensitive to blur but struggle to effectively recognize outliers within the scene, while mask-transformer-based methods tend to produce false positives. POS achieves a good balance, with mean AuPRC and FPR₉₅ improvements of approximately 24% and 13%, respectively, on the two benchmarks.

In Fig. 13, we visualize the *PanOoS* results produced by POS and other mask-transformer-based methods. Notably, POS effectively suppresses false positives in background regions, especially at the boundaries separating inliers, while better preserving the smoothness of the outlier map compared to other methods,

| Method | AuPRC | FPR ₉₅ |
|-------------------|--------------|-------------------|
| PEBAL [29] | 62.37 | 28.29 |
| DenseHybrid [30] | - | - |
| EAM [23] | 69.40 | 7.70 |
| Mask2Anomaly [25] | 79.70 | 13.45 |
| RbA [24] | <u>85.42</u> | <u>6.92</u> |
| Ours | 89.39 | 6.25 |

TABLE 4: **Pinhole out-of-distribution segmentation results** on Road Anomaly. The best and second best results are **bold** and underlined, respectively; “-” indicates the unavailability of benchmark results.

despite sharing the same mask classification training paradigm. Benefiting from the generalization ability of vision-language model, Prompt-based Restoration Attention (PRA) and Bilevel Prompt Distribution Learning (BPDL), POS performs excellently on the two benchmarks for *PanOoS*, perfectly adapting to the background clutter and pixel distortions caused by the broader FoV of panoramic images.

5.5 Results of Pinhole Out-of-distribution Segmentation

To further investigate the segmentation capacity of the proposed POS in the pinhole domain, we evaluate its *OoS* performance on one standard pinhole-*OoS* datasets [49]. During the outlier exposure fine-tuning, we do not apply panoramic-oriented disentanglement and fine-tune only the MLP and the linear layers. The results in Table 4 indicate that POS excels on Road Anomaly, and achieves precise segmentation of outliers with minimal false positives.

5.6 Ablation Study

In this section, we conduct comprehensive ablation experiments to validate the effectiveness of our solution. To ensure a rigorous comparison, all the results reported in this section are based on the DenseOoS benchmark.

Each Component in POS. Table 5 presents the component-wise ablation results of the technical novelties included in POS. Using the image encoder alone as the backbone, the model demonstrates strong potential for omnidirectional visual perception. However, it still struggles with semantic ambiguity and background interference in complex panoramic scenes. By incorporating Prompt-based Restoration Attention (PRA), the model significantly improves pixel-level semantic associations through prompt distribution learning, enhancing panoramic perception. This results in an

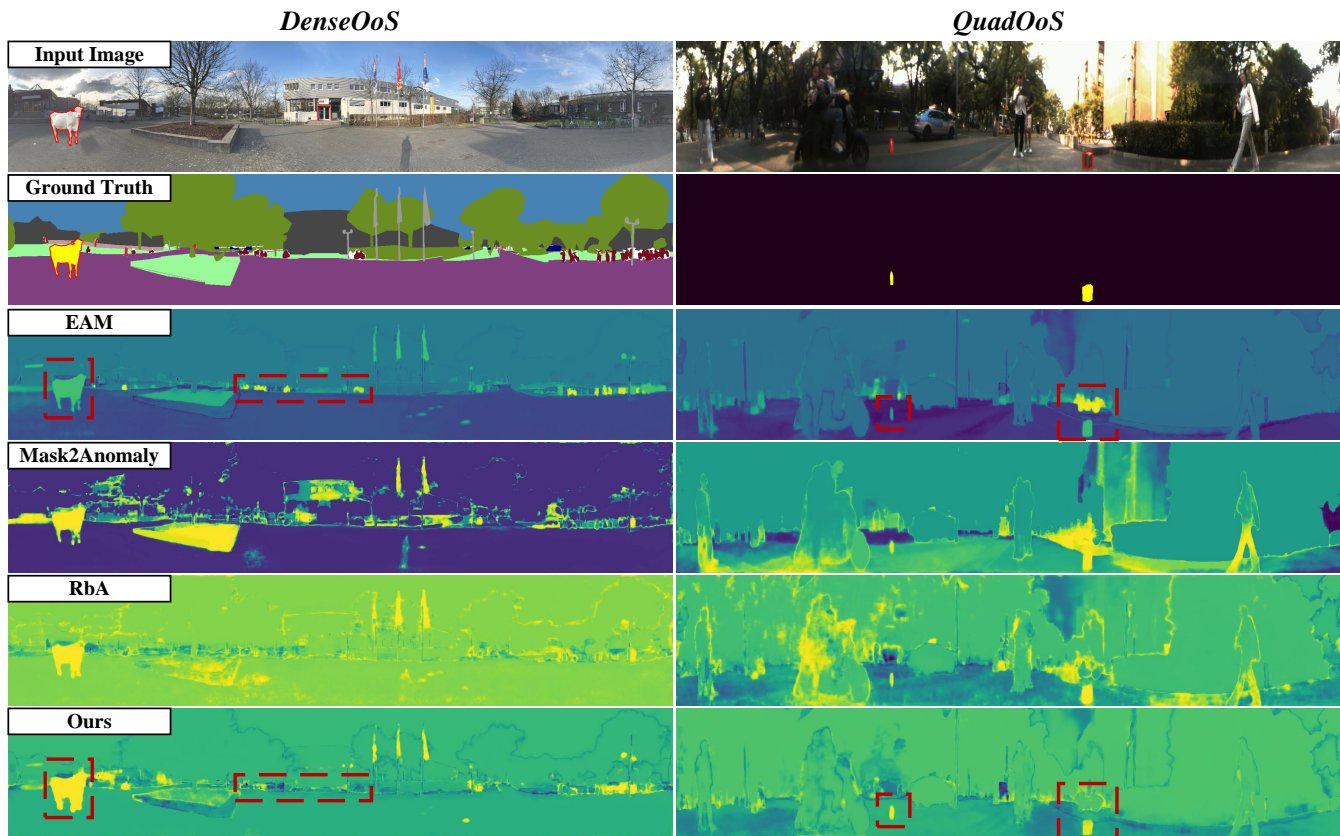


Fig. 13: **Visual comparisons of *PanOoS***. We observe that when existing pinhole-*OoS* methods are transferred to *PanOoS*, current state-of-the-art methods generally struggle with misidentifying complex background as outliers. Although EAM [23] has a low false positive rate, it incorrectly identifies bicycles as outliers and nearly overlooks the actual outliers. In contrast, Mask2Anomaly [25] and RbA [24] suffer from large false positives in the background region, whereas POS delivers more precise *PanOoS* across the 360°.

| PRA | BPDL | AuPRC | FPR ₉₅ | mIoU |
|-----|------|--------------|-------------------|--------------|
| | | 76.88 | 0.84 | 61.73 |
| ✓ | | 83.94 | 0.46 | 62.50 |
| ✓ | ✓ | 85.56 | 0.45 | 63.30 |

TABLE 5: **Component-wise ablation study of POS**. PRA: Prompt-based Restoration Attention; BPDL: Bilevel Prompt Distribution Learning.

increase in AuPRC to 83.94% (+7.06%) and an improvement in mIoU to 62.50% (+0.77%), highlighting the effectiveness in mitigating dense pixel semantic blurring. Further incorporation of Bilevel Prompt Distribution Learning (BPDL) leads to a synergistic optimization: PRA enhances inter-class discrimination through semantic decoupling, while BPDL preserves topological consistency via manifold learning. This combined mechanism enables the model to achieve groundbreaking performance in the *PanOoS* task: 85.56% AuPRC, 0.45% FPR₉₅, and 63.30% mIoU. Not only does it overcome the coupling challenges of semantic ambiguity and geometric distortion that traditional pinhole-*OoS* methods cannot deal with, but it also establishes a new benchmark for panoramic scene understanding.

Prompt-base Restoration Attention. To better understand the effect of Prompt-based Restoration Attention (PRA), we perform an ablation analysis of its structure in Table 6. Experimental

| MA | CA | SAC | AuPRC | FPR ₉₅ | mIoU |
|----|----|-----|--------------|-------------------|--------------|
| ✓ | | | 81.24 | 0.67 | 58.03 |
| ✓ | ✓ | | 81.98 | 0.53 | 62.48 |
| ✓ | ✓ | ✓ | 85.56 | 0.45 | 63.30 |

TABLE 6: **Structural ablation of Prompt-based Restoration Attention**. MA: Masked Attention; CA: Cross Attention; SAC: Self-adaptive Correction.

results show that the simple use of Masked Attention (MA), which only interacts with image features, cannot adapt to the characteristics of panoramic images, resulting in poor performance across almost all metrics. This demonstrates that prompt-based Cross Attention (CA) effectively captures high-level semantic interactions, alleviating the impact of pixel distortions on semantic decoding. Furthermore, to prevent blind confidence during the learning process, the proposed Self-adaptive Correction (SAC) dynamically adjusts the semantic confidence for each query, leading to more accurate semantic segmentation and avoiding excessively high voting scores for out-of-distribution areas. This is visually substantiated in Fig. 14, where the inter-query attention maps after three stages explicitly manifest the effectiveness of PRA for hierarchical semantic refinement.

Bilevel Prompt Distribution Learning. The proposed BPDL belongs to the domain of metric learning. Unlike traditional methods

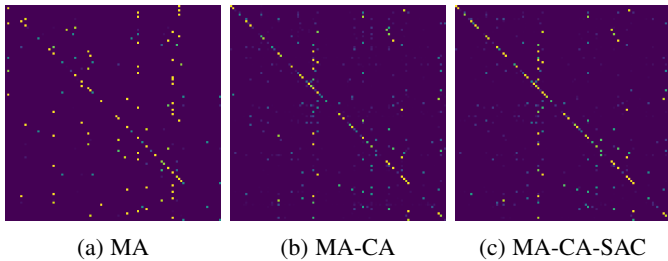


Fig. 14: **Attention maps of queries** in PRA after different query stages, resembling a confusion matrix in which each query has the highest semantic similarity with itself. When querying only with image features, the query semantic information is relatively vague. However, after further interaction with the prompt embeddings, the semantics become clearer, and the self-adaptive correction further mitigates the impact of pixel distortion on semantic decoding.

that rely on manually defined or learned centroid embeddings as class prototypes, BPDFL uses semantically rich text embeddings as prototypes. This approach allows for a coarse-grained predefinition of distribution regions for each class. Moreover, BPDFL utilizes a bilevel learning framework for distribution optimization: the lower-level optimization refines the inter-class distributions for known classes, while the upper-level optimization adjusts the global distribution space. As shown in Table 7, each component of the \mathcal{L}_{bpdf} contributes to spatial distribution optimization, with the \mathcal{L}_{ind} and \mathcal{L}_{pixel} loss terms leading to particularly notable performance gains (AuPRC: +2.95%/+2.48%, mIoU: +0.63%/+0.41%). Ablation experiments confirm that integrating all loss components results in optimal performance across all evaluation metrics.

As outlined in Eqs. 9, 18, 19, and 24, the BPDFL framework involves four key hyperparameters: inter-class margin s , distribution margin d , loss weight of \mathcal{L}_{Dis} α , and balancing coefficient λ_{bpdf} . The inter-class margin s controls the trade-off between intra-class embedding compactness and inter-class separability, while the distribution margin d governs the geometric structure of the embedding space. The parameter α adjusts the relative contribution of the \mathcal{L}_{Dis} loss, and λ_{bpdf} balances the weights between the \mathcal{L}_{bpdf} loss and other loss terms. Through a systematic sensitivity analysis (Fig. 15), we observe a notable convex trend for the s . Both mIoU and AuPRC exhibit convex behavior as functions of s , while FPR_{95} shows a concave trend but remains stable within a fluctuation range of 0.03%. Similarly, the distribution margin d follows a similar optimization trend, confirming the synergistic effect of the bilevel distribution constraints. The parameter α regulates the distance between the upper-level class prototype embeddings and the distribution embeddings, enhancing the isolation of out-of-distribution embeddings. However, an excessive emphasis on this constraint can reduce closed-set semantic segmentation performance. Additionally, when λ_{bpdf} exceeds a certain threshold (0.01), the model tends to focus too much on the out-of-distribution detection task, leading to significant degradation in closed-set segmentation performance (with mIoU decreasing by 0.6%), while out-of-distribution detection metrics remain relatively stable.

Outlier Exposure Fine-tuning. We further empirically evaluate the impact of fine-tuning parameters during the optimization of the prompt distribution space. As shown in Table 8a, performance evaluations on the DenseOoS dataset for PanOoS demonstrate

| \mathcal{L}_{pixel} | \mathcal{L}_{ind} | \mathcal{L}_{inDir} | $\mathcal{L}_{outlier}$ | AuPRC | FPR ₉₅ | mIoU |
|-----------------------|---------------------|-----------------------|-------------------------|--------------|-------------------|--------------|
| ✓ | | | | 81.72 | 0.54 | 62.69 |
| ✓ | | ✓ | | 82.61 | 0.50 | 62.67 |
| ✓ | ✓ | | ✓ | 83.61 | 0.49 | 63.04 |
| ✓ | ✓ | ✓ | | 83.37 | 0.49 | 63.06 |
| ✓ | ✓ | ✓ | ✓ | 83.08 | 0.50 | 62.89 |
| ✓ | ✓ | ✓ | ✓ | 85.56 | 0.45 | 63.30 |

TABLE 7: **Ablation study of different loss contributions** in bilevel prompt distribution learning loss \mathcal{L}_{bpdf} .

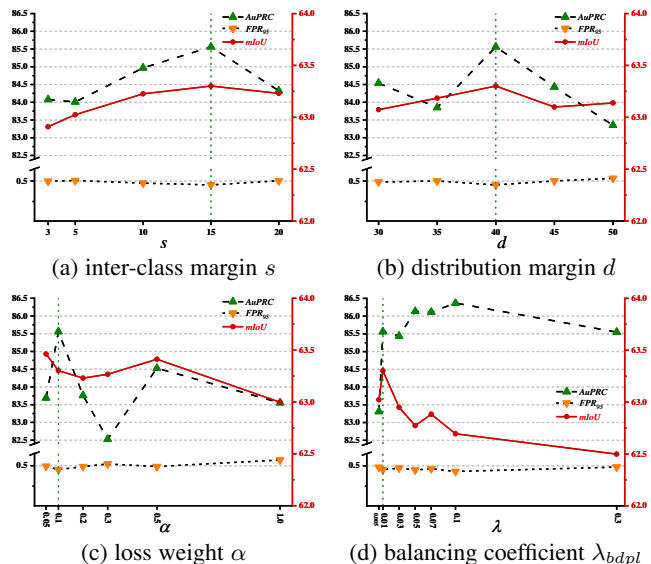


Fig. 15: **Experiments of different settings of s , d , α and λ_{bpdf} .**

that the model reaches optimal performance after approximately 30k iterations, after which overfitting begins. For the outlier data exposure control parameter p_{out} , experiments reveal that when $p_{out} > 0.3$, both closed-set performance and out-of-distribution segmentation performance deteriorate. Based on these results, we selected 0.3 as the optimal value, balancing outlier detection with closed-set performance.

Moreover, a comparison of fine-tuning strategies (see Table 8c) shows that the panoramic-oriented disentanglement (Pixel Dec.) outperforms other strategies. Specifically, fine-tuning only the MLP and linear layers (*w/o*) or the Transformer decoder (Trans. Dec.) fails to effectively address the complexities of panoramic images. While additional fine-tuning of all decoders performs comparably in FPR_{95} , it does not achieve optimal results on AuPRC and mIoU, decreasing segmentation accuracy. This suggests that excessive fine-tuning can introduce semantic ambiguity, compromising segmentation accuracy. These findings verify the effectiveness of our proposed fine-tuning strategy in preserving semantic consistency and enhancing out-of-distribution detection.

Features and layers in Transformer Decoder. To further analyze the most favorable settings for PanOoS, we conduct additional ablation experiments on the decoded features and corresponding number of layers in Transformer decoder. As shown in Table 9, the results align with previous work: by decoding only semantically rich features and reducing the number of decoder layers, semantic confusion can be effectively alleviated, which helps to better align the logit scores and results in better outlier performance [24]. Specialized object queries perform worse with more decoder

| Num Iter | AuPRC | FPR ₉₅ | mIoU | p_{out} | AuPRC | FPR ₉₅ | mIoU | Module | AuPRC | FPR ₉₅ | mIoU |
|----------|--------------|-------------------|--------------|-----------|--------------|-------------------|--------------|-------------|--------------|-------------------|--------------|
| 15k | 79.19 | 0.49 | 57.49 | 0.1 | 86.30 | 0.45 | 62.47 | | | | |
| 20k | 78.22 | 0.57 | 60.14 | 0.2 | 85.72 | 0.45 | 62.73 | w/o | 55.66 | 7.44 | 54.11 |
| 25k | 84.04 | 0.51 | 62.71 | 0.3 | 85.56 | 0.45 | 63.30 | Decoders | 84.25 | 0.50 | 62.38 |
| 30k | 85.56 | 0.45 | 63.30 | 0.4 | 81.28 | 0.59 | 62.17 | Pixel Dec. | 85.56 | 0.45 | 63.30 |
| 35k | 82.08 | 0.56 | 63.14 | 0.5 | 80.97 | 0.53 | 62.36 | Trans. Dec. | 46.91 | 5.58 | 57.89 |

(a) Number of iterations

(b) Outlier selection probability

(c) Different fine-tuning strategies

TABLE 8: Ablation study on outlier exposure fine-tuning.

| Features | Layer | AuPRC | FPR ₉₅ | mIoU |
|-----------------|-------|--------------|-------------------|--------------|
| f_4 | 1 | 85.56 | 0.45 | 63.30 |
| | 3 | 71.18 | 0.68 | 57.72 |
| | 6 | 76.46 | 0.64 | 57.33 |
| f_2, f_3, f_4 | 3 | 72.38 | 0.94 | 58.96 |
| | 6 | 63.60 | 1.01 | 58.66 |
| | 9 | 65.91 | 1.06 | 58.79 |

TABLE 9: Comparison of different features in Transformer Decoder. The f_2 and f_3 are feature maps with stride $8(c_8)$ and $16(c_{16})$ processed by DeformAttn layers, respectively.

layers. This also supports our view that, while ensuring semantic clarity, enhancing the model’s perception of panoramic pixels can significantly improve the performance of *PanOoS*.

6 CONCLUSION

In this work, we introduce a novel task, termed *Panoramic Out-of-distribution Segmentation (PanOoS)*, which aims to enhance panoramic holistic scene understanding. To address *PanOoS*, we propose the first panoramic out-of-distribution segmentation solution, POS, which effectively tackles the challenges posed by panoramas, including pixel distortions and background clutter. The proposed PRA optimizes the interaction between visual features and text embeddings, significantly improving semantic understanding in complex panoramic scenes and mitigating semantic confusion. The BPDFL further strengthens the model’s ability to recognize out-of-distribution regions by optimizing the embedding space in a hierarchical manner. The synergistic combination of PRA and BPDFL allows POS to effectively resolve issues related to semantic ambiguity and geometric distortion in panoramic images. Moreover, we establish DenseOoS and QuadOoS benchmarks to facilitate the optimization and evaluation of *PanOoS* models, paving the way for future research in *PanOoS*. Extensive experiments on these two benchmarks demonstrate that POS achieves state-of-the-art performance in *PanOoS*, significantly improving segmentation accuracy, robustness, and the detection of out-of-distribution regions.

In the future, we intend to incorporate multimodal fusion techniques, combining various scene information types (e.g., depth and point clouds) to boost the model’s adaptability to defocus and motion blur. Additionally, incorporating time series information to strengthen the scene perception capabilities in dynamic environments is worth investigating to further improve *PanOoS* performance, with the aim of adapting to complex dynamic conditions, as well as open-set and 3D perception tasks.

ACKNOWLEDGMENTS

This work was supported in part by the National Natural Science Foundation of China under Grant No. U21A20518, No. U23A20341, and No. 62473139.

REFERENCES

- [1] Z. Shen, C. Lin, K. Liao, L. Nie, Z. Zheng, and Y. Zhao, “PanoFormer: Panorama transformer for indoor 360° depth estimation,” in *ECCV*, 2022.
- [2] Z. Ling, Z. Xing, X. Zhou, M. Cao, and G. Zhou, “PanoSwin: a panostyle swin transformer for panorama understanding,” in *CVPR*, 2023.
- [3] H. Yu, L. He, B. Jian, W. Feng, and S. Liu, “PanelNet: Understanding 360 indoor environment via panel representation,” in *CVPR*, 2023.
- [4] C. Zhang *et al.*, “DeepPanoContext: Panoramic 3D scene understanding with holistic scene context graph and relation-based optimization,” in *ICCV*, 2021.
- [5] Z. Teng *et al.*, “360BEV: Panoramic semantic mapping for indoor bird’s-eye view,” in *WACV*, 2024.
- [6] J. Zheng *et al.*, “Open panoramic segmentation,” in *ECCV*, 2024.
- [7] K. Yang, X. Hu, L. M. Bergasa, E. Romera, and K. Wang, “PASS: Panoramic annular semantic segmentation,” *IEEE Transactions on Intelligent Transportation Systems*, 2020.
- [8] J. Zhang, K. Yang, C. Ma, S. Reiß, K. Peng, and R. Stiefelwagen, “Bending reality: Distortion-aware transformers for adapting to panoramic semantic segmentation,” in *CVPR*, 2022.
- [9] X. Zheng, J. Zhu, Y. Liu, Z. Cao, C. Fu, and L. Wang, “Both style and distortion matter: Dual-path unsupervised domain adaptation for panoramic semantic segmentation,” in *CVPR*, 2023.
- [10] Y. Cao *et al.*, “Occlusion-aware seamless segmentation,” in *ECCV*, 2024.
- [11] X. Zheng, T. Pan, Y. Luo, and L. Wang, “Look at the neighbor: Distortion-aware unsupervised domain adaptation for panoramic semantic segmentation,” in *ICCV*, 2023.
- [12] W. Zhang, Y. Liu, X. Zheng, and L. Wang, “GoodSAM: Bridging domain and capacity gaps via segment anything model for distortion-aware panoramic semantic segmentation,” in *CVPR*, 2024.
- [13] H. Ai, Z. Cao, and L. Wang, “A survey of representation learning, optimization strategies, and applications for omnidirectional vision,” *International Journal of Computer Vision*, 2025.
- [14] M. Cordts *et al.*, “The cityscapes dataset for semantic urban scene understanding,” in *CVPR*, 2016.
- [15] S. Minaee, Y. Boykov, F. Porikli, A. Plaza, N. Kehtarnavaz, and D. Terzopoulos, “Image segmentation using deep learning: A survey,” *IEEE Transactions on Pattern Analysis and Machine Intelligence*, 2022.
- [16] W. Wang, T. Zhou, F. Yu, J. Dai, E. Konukoglu, and L. Van Gool, “Exploring cross-image pixel contrast for semantic segmentation,” in *ICCV*, 2021.
- [17] C. Ma, J. Zhang, K. Yang, A. Roitberg, and R. Stiefelwagen, “DensePASS: Dense panoramic semantic segmentation via unsupervised domain adaptation with attention-augmented context exchange,” in *ITSC*, 2021.
- [18] S. Gao, K. Yang, H. Shi, K. Wang, and J. Bai, “Review on panoramic imaging and its applications in scene understanding,” *IEEE Transactions on Instrumentation and Measurement*, 2022.
- [19] K. Yang, J. Zhang, S. Reiß, X. Hu, and R. Stiefelwagen, “Capturing omni-range context for omnidirectional segmentation,” in *CVPR*, 2021.
- [20] X. Li, T. Wu, Z. Qi, G. Wang, Y. Shan, and X. Li, “SGAT4PASS: Spherical geometry-aware transformer for panoramic semantic segmentation,” in *IJCAI*, 2023.
- [21] A. Jaus, K. Yang, and R. Stiefelwagen, “Panoramic panoptic segmentation: Insights into surrounding parsing for mobile agents via unsupervised contrastive learning,” *IEEE Transactions on Intelligent Transportation Systems*, 2023.
- [22] W. Zhang, Y. Liu, X. Zheng, and L. Wang, “GoodSAM++: Bridging domain and capacity gaps via segment anything model for panoramic semantic segmentation,” *arXiv preprint arXiv:2408.09115*, 2024.
- [23] M. Grcic, J. Saric, and S. Segvic, “On advantages of mask-level recognition for outlier-aware segmentation,” in *CVPRW*, 2023.
- [24] N. Nayal, M. Yavuz, J. F. Henriques, and F. Güney, “RbA: Segmenting unknown regions rejected by all,” in *ICCV*, 2023.
- [25] S. N. Rai, F. Cermelli, B. Caputo, and C. Masone, “Mask2Anomaly: Mask transformer for universal open-set segmentation,” *IEEE Transactions on Pattern Analysis and Machine Intelligence*, 2024.

- [26] B. Cheng, I. Misra, A. G. Schwing, A. Kirillov, and R. Girdhar, “Masked-attention mask transformer for universal image segmentation,” in *CVPR*, 2022.
- [27] Q. Yu, J. He, X. Deng, X. Shen, and L.-C. Chen, “Convolutions die hard: Open-vocabulary segmentation with single frozen convolutional CLIP,” in *NeurIPS*, 2023.
- [28] A. Radford *et al.*, “Learning transferable visual models from natural language supervision,” in *ICML*, 2021.
- [29] Y. Tian, Y. Liu, G. Pang, F. Liu, Y. Chen, and G. Carneiro, “Pixel-wise energy-biased abstention learning for anomaly segmentation on complex urban driving scenes,” in *ECCV*, 2022.
- [30] M. Grcic, P. Bevandic, and S. Segvic, “DenseHybrid: Hybrid anomaly detection for dense open-set recognition,” in *ECCV*, 2022.
- [31] L. Hoyer, D. Dai, and L. Van Gool, “DAFormer: Improving network architectures and training strategies for domain-adaptive semantic segmentation,” in *CVPR*, 2022.
- [32] J. Zhang *et al.*, “Behind every domain there is a shift: Adapting distortion-aware vision transformers for panoramic semantic segmentation,” *IEEE Transactions on Pattern Analysis and Machine Intelligence*, 2024.
- [33] Q. Jiang *et al.*, “Minimalist and high-quality panoramic imaging with PSF-aware transformers,” *IEEE Transactions on Image Processing*, 2024.
- [34] Y. Xu, K. Wang, K. Yang, D. Sun, and J. Fu, “Semantic segmentation of panoramic images using a synthetic dataset,” in *SPIE*, 2019.
- [35] S. Orhan and Y. Bastanlar, “Semantic segmentation of outdoor panoramic images,” *Signal, Image and Video Processing*, 2022.
- [36] J. Kim, S. Jeong, and K. Sohn, “PASTS: Toward effective distilling transformer for panoramic semantic segmentation,” in *ICIP*, 2022.
- [37] S. Guttikonda and J. Rambach, “Single frame semantic segmentation using multi-modal spherical images,” in *WACV*, 2024.
- [38] S. Jang, J. Na, and D. Oh, “DaDA: Distortion-aware domain adaptation for unsupervised semantic segmentation,” in *NeurIPS*, 2022.
- [39] J. Zhu, H. Bai, and L. Wang, “Patch-Mix transformer for unsupervised domain adaptation: A game perspective,” in *CVPR*, 2023.
- [40] J. Zhang, C. Ma, K. Yang, A. Roitberg, K. Peng, and R. Stiefelhagen, “Transfer beyond the field of view: Dense panoramic semantic segmentation via unsupervised domain adaptation,” *IEEE Transactions on Intelligent Transportation Systems*, 2022.
- [41] J. Jiang, J. Zhu, Z. Xu, X. Chen, S. Zhao, and H. Yao, “Gaussian constrained diffeomorphic deformation network for panoramic semantic segmentation,” in *ICASSP*, 2025.
- [42] Z. Yuan, J. Wang, Y. Lv, D. Wang, and Y. Fang, “Laformer: Vision transformer for panoramic image semantic segmentation,” *IEEE Signal Processing Letters*, 2023.
- [43] M. Liu, S. Wang, Y. Guo, Y. He, and H. Xue, “Pano-SfMLearner: Self-supervised multi-task learning of depth and semantics in panoramic videos,” *IEEE Signal Processing Letters*, 2021.
- [44] J. Jiang *et al.*, “Multi-source domain adaptation for panoramic semantic segmentation,” *Information Fusion*, 2025.
- [45] X. Zheng, P. Zhou, A. V. Vasilakos, and L. Wang, “Semantics, distortion, and style matter: Towards source-free UDA for panoramic segmentation,” in *CVPR*, 2024.
- [46] —, “360SFUDA++: Towards source-free UDA for panoramic segmentation by learning reliable category prototypes,” *IEEE Transactions on Pattern Analysis and Machine Intelligence*, 2024.
- [47] D. Zhong *et al.*, “OmniSAM: Omnidirectional segment anything model for uda in panoramic semantic segmentation,” *arXiv preprint arXiv:2503.07098*, 2025.
- [48] R. Chan *et al.*, “SegmentMelfYouCan: A benchmark for anomaly segmentation,” in *NeurIPS*, 2021.
- [49] K. Lis, K. Nakka, P. Fua, and M. Salzmann, “Detecting the unexpected via image resynthesis,” in *ICCV*, 2019.
- [50] H. Blum, P.-E. Sarlin, J. Nieto, R. Siegwart, and C. Cadena, “The fishyscapes benchmark: Measuring blind spots in semantic segmentation,” *International Journal of Computer Vision*, 2021.
- [51] J. Mukhoti and Y. Gal, “Evaluating bayesian deep learning methods for semantic segmentation,” *arXiv preprint arXiv:1811.12709*, 2018.
- [52] C. Corbière, N. Thome, A. Bar-Hen, M. Cord, and P. Pérez, “Addressing failure prediction by learning model confidence,” in *NeurIPS*, 2019.
- [53] D. Hendrycks *et al.*, “Scaling out-of-distribution detection for real-world settings,” *arXiv preprint arXiv:1911.11132*, 2019.
- [54] S. Jung, J. Lee, D. Gwak, S. Choi, and J. Choo, “Standardized max logits: A simple yet effective approach for identifying unexpected road obstacles in urban-scene segmentation,” in *ICCV*, 2021.
- [55] J. Cen, P. Yun, J. Cai, M. Y. Wang, and M. Liu, “Deep metric learning for open world semantic segmentation,” in *ICCV*, 2021.
- [56] Y. Xia, Y. Zhang, F. Liu, W. Shen, and A. L. Yuille, “Synthesize then compare: Detecting failures and anomalies for semantic segmentation,” in *ECCV*, 2020.
- [57] D. Haldimann, H. Blum, R. Siegwart, and C. Cadena, “This is not what I imagined: Error detection for semantic segmentation through visual dissimilarity,” *arXiv preprint arXiv:1909.00676*, 2019.
- [58] T. Vojir, T. Sipka, R. Aljundi, N. Chumerin, D. O. Reino, and J. Matas, “Road anomaly detection by partial image reconstruction with segmentation coupling,” in *ICCV*, 2021.
- [59] M. Grcic, P. Bevandic, Z. Kalafatic, and S. Segvic, “Dense anomaly detection by robust learning on synthetic negative data,” *arXiv preprint arXiv:2112.12833*, 2021.
- [60] K. Lis, S. Honari, P. Fua, and M. Salzmann, “Detecting road obstacles by erasing them,” *IEEE Transactions on Pattern Analysis and Machine Intelligence*, 2024.
- [61] D. Fontanel, F. Cermelli, M. Mancini, and B. Caputo, “Detecting anomalies in semantic segmentation with prototypes,” in *CVPRW*, 2021.
- [62] R. Chan, M. Rottmann, and H. Gottschalk, “Entropy maximization and meta classification for out-of-distribution detection in semantic segmentation,” in *ICCV*, 2021.
- [63] Y. Liu *et al.*, “Residual pattern learning for pixel-wise out-of-distribution detection in semantic segmentation,” in *ICCV*, 2023.
- [64] H. Choi, H. Jeong, and J. Y. Choi, “Balanced energy regularization loss for out-of-distribution detection,” in *CVPR*, 2023.
- [65] D. Hendrycks, M. Mazeika, and T. Dietterich, “Deep anomaly detection with outlier exposure,” *arXiv preprint arXiv:1812.04606*, 2018.
- [66] J. Deng, W. Dong, R. Socher, L.-J. Li, K. Li, and L. Fei-Fei, “ImageNet: A large-scale hierarchical image database,” in *CVPR*, 2009.
- [67] T. Lin *et al.*, “Microsoft COCO: Common objects in context,” in *ECCV*, 2014.
- [68] B. Zhou, H. Zhao, X. Puig, S. Fidler, A. Barriuso, and A. Torralba, “Scene parsing through ADE20K dataset,” in *CVPR*, 2017.
- [69] J. Ackermann, C. Sakaridis, and F. Yu, “Maskomaly: Zero-shot mask anomaly segmentation,” in *BMVC*, 2023.
- [70] A. Delic, M. Grcic, and S. Segvic, “Outlier detection by ensembling uncertainty with negative objectness,” in *BMVC*, 2024.
- [71] H. Zhang, F. Li, L. Qi, M.-H. Yang, and N. Ahuja, “CSL: Class-agnostic structure-constrained learning for segmentation including the unseen,” in *AAAI*, 2024.
- [72] Y. Shoeb, A. Nowzad, and H. Gottschalk, “Out-of-distribution segmentation in autonomous driving: Problems and state of the art,” *arXiv preprint arXiv:2503.08695*, 2025.
- [73] Z. Liu, H. Mao, C.-Y. Wu, C. Feichtenhofer, T. Darrell, and S. Xie, “A ConvNet for the 2020s,” in *CVPR*, 2022.
- [74] X. Zhu, W. Su, L. Lu, B. Li, X. Wang, and J. Dai, “Deformable DETR: Deformable transformers for end-to-end object detection,” in *ICLR*, 2021.
- [75] T. Lin, P. Dollár, R. B. Girshick, K. He, B. Hariharan, and S. J. Belongie, “Feature pyramid networks for object detection,” in *CVPR*, 2017.
- [76] X. He, Y. Zhou, Z. Zhou, S. Bai, and X. Bai, “Triplet-center loss for multi-view 3D object retrieval,” in *CVPR*, 2018.
- [77] Z.-g. Liu, Y.-m. Fu, Q. Pan, and Z.-w. Zhang, “Orientational distribution learning with hierarchical spatial attention for open set recognition,” *IEEE Transactions on Pattern Analysis and Machine Intelligence*, 2023.
- [78] F. Milletari, N. Navab, and S.-A. Ahmadi, “V-Net: Fully convolutional neural networks for volumetric medical image segmentation,” in *3DV*, 2016.
- [79] T. Loiseau, T. Vu, M. Chen, P. Pérez, and M. Cord, “Reliability in semantic segmentation: Can we use synthetic data?” in *ECCV*, 2024.
- [80] P. de Jorge, R. Volpi, P. K. Dokania, P. H. S. Torr, and G. Rogez, “Placing objects in context via inpainting for out-of-distribution segmentation,” in *ECCV*, 2024.
- [81] G. Neuhold, T. Ollmann, S. R. Bulò, and P. Kotschieder, “The mapillary vistas dataset for semantic understanding of street scenes,” in *ICCV*, 2017.
- [82] G. Ilharco *et al.*, “OpenCLIP,” 2021.
- [83] C. Schuhmann *et al.*, “LAION-5B: An open large-scale dataset for training next generation image-text models,” in *NeurIPS*, 2022.

APPENDIX A METHODOLOGY

A.1 Prompt Templates

We adopt the prompt templates from [27], [28], but make additional prompt optimization to describe the different distribution items more accurately. Specifically, the lists of templates for class and distribution prompts are as follows:

Class:

“A photo of a {}.”
 “This is a photo of a {}.”
 “There is a {} in the scene.”
 “There is the {} in the scene.”
 “A photo of a {} in the scene.”
 “A photo of a small {}.”
 “A photo of a medium {}.”
 “A photo of a large {}.”
 “This is a photo of a small {}.”
 “This is a photo of a medium {}.”
 “This is a photo of a large {}.”
 “There is a small {} in the scene.”
 “There is a medium {} in the scene.”
 “There is a large {} in the scene.”

Distribution:

“A photo of an {} item.”
 “This is a photo of an {} item.”
 “There is an {} item in the urban or rural scene.”
 “There is the {} item in the urban or rural scene.”
 “A photo of an {} item in the urban or rural scene.”
 “A photo of a small {} item.”
 “A photo of a medium {} item.”
 “A photo of a large {} item.”
 “This is a photo of a small {} item.”
 “This is a photo of a medium {} item.”
 “This is a photo of a large {} item.”
 “There is a small {} item in the urban or rural scene.”
 “There is a medium {} item in the urban or rural scene.”
 “There is a large {} item in the urban or rural scene.”

APPENDIX B BENCHMARKS AND EXPERIMENTS

B.1 More Details of Datasets

As shown in Table B.1, we present the specific types of outliers in DenseOoS. DenseOoS is based on the designs in POC [80] and additionally includes 5 other common anomalous objects (cattle, duck, cock, box, and rock). In addition, we also list some types of outliers in QuadOoS. As present in Fig. B.1, the outliers mainly consist of two parts: human-defined and existing in the neighborhood.

B.2 Comparative Experiments

For the experiments on *PanOoS*, we compare POS to the state-of-the-art pinhole-*OoS* methods: per-pixel architecture [29], [30] and mask-transformer-based [23], [24], [25] methods, using the models that were shared in their respective repositories.

| Class | ID | Number |
|--------------------------------|----|--------|
| stroller | 19 | 19 |
| trolley | 20 | 20 |
| garbage bag | 21 | 55 |
| wheelie bin | 22 | 41 |
| suitcase | 23 | 16 |
| skateboard | 24 | 13 |
| chair dumped on the street | 25 | 23 |
| sofa dumped on the street | 26 | 41 |
| furniture dumped on the street | 27 | 32 |
| mattress dumped on the street | 28 | 63 |
| garbage dumped on the street | 29 | 90 |
| clothes dumped on the street | 30 | 101 |
| cement mixer on the street | 31 | 48 |
| cat | 32 | 10 |
| dog | 33 | 10 |
| bird flying | 34 | 10 |
| horse | 35 | 34 |
| skunk | 36 | 38 |
| sheep | 37 | 48 |
| crocodile | 38 | 19 |
| alligator | 39 | 12 |
| bear | 40 | 65 |
| llama | 41 | 18 |
| tiger | 42 | 38 |
| monkey | 43 | 7 |
| cattle | 44 | 43 |
| duck | 45 | 28 |
| cock | 46 | 12 |
| box | 47 | 25 |
| rock | 48 | 21 |
| total | - | 1000 |

TABLE B.1: Details of the DenseOoS dataset.



Fig. B.1: Examples of outliers included in the QuadOoS dataset. Including but not limited to the above types.

APPENDIX C MORE QUANTITATIVE RESULTS

C.1 More in-distribution segmentation results

To provide a thorough analysis of the panoramic segmentation and demonstrate that excellent closed-set segmentation performance ensures effective out-of-distribution segmentation, we present the accuracy results for each inlier class in the DenseOoS dataset, as shown in Table C.1. To benchmark our model, we conduct a comparative study with the previous state-of-the-art panoramic semantic segmentation methods, namely DAFormer [31], Trans4PASS [8], Trans4PASS+ [32], and 360SFUDA++ [46]. DAFormer introduces domain-adaptive transformers to improve semantic segmentation across domains.

| Method | road | sidewalk | building | wall | fence | pole | traffic light | traffic sign | vegetation | terrain | sky | person | rider | car | truck | bus | train | motorcycle | bicycle | Metric |
|----------------------|--------------|--------------|--------------|--------------|--------------|--------------|---------------|--------------|--------------|--------------|--------------|--------------|--------------|--------------|--------------|--------------|--------------|--------------|--------------|--------------|
| DAFormer [31] | 48.94 | 31.78 | 84.12 | 26.51 | 31.06 | 24.92 | 6.83 | 7.73 | 71.86 | 40.63 | 91.23 | 44.13 | 2.1 | 78.02 | 55.02 | 25.24 | 84.89 | 61.37 | 29.59 | 44.53 |
| Trans4PASS (S) [8] | 74.28 | 30.68 | 84.79 | 28.45 | 36.60 | 27.90 | 15.40 | 15.11 | 78.99 | 33.71 | 93.28 | 49.69 | 6.79 | 82.00 | 46.42 | 51.79 | 72.84 | 68.34 | 40.63 | 49.35 |
| Trans4PASS+ (S) [32] | 74.74 | 34.17 | 85.43 | 23.46 | 42.78 | 28.45 | 17.14 | 18.08 | 79.64 | 29.41 | 93.00 | 48.74 | 5.40 | 82.76 | 50.54 | 44.91 | 91.49 | 61.49 | 40.20 | 50.11 |
| 360SFUDA++ [46] | 72.29 | 45.24 | 84.91 | 32.11 | 38.18 | 29.83 | 19.28 | 17.98 | 76.02 | 27.23 | 92.01 | 53.14 | 18.74 | 81.35 | 44.42 | 45.38 | 82.84 | 60.93 | 36.92 | 50.46 |
| Ours | 87.67 | 59.56 | 89.68 | 50.88 | 45.10 | 42.62 | 34.02 | 22.73 | 81.21 | 45.19 | 94.59 | 72.24 | 14.42 | 86.62 | 64.88 | 69.16 | 95.27 | 82.98 | 63.92 | 63.30 |

TABLE C.1: **Panoramic semantic segmentation results** on the DenseOoS benchmark. The per-class results are reported as IoU, and the metric is mIoU.

Trans4PASS and its enhanced variant, Trans4PASS+, employ transformer-based architectures specifically designed to mitigate distortions and exploit contextual dependencies in panorama. 360SFUDA++ represents an advanced source-free domain adaptation framework based on self-training, tailored to panoramic scenarios. While these methods achieve good performance under closed-set conditions, they experience notable degradation in the presence of out-of-distribution regions, owing to their limited generalization beyond the predefined semantic space. This limitation underscores the importance of enhancing robustness to unexpected content in real-world panoramic scenes.

As shown in the experimental results, our model achieves a significant mIoU of 63.30%, surpassing the performance of the previous best model by a large margin of 12.84%. A detailed breakdown of per-class performance reveals that our model excels across numerous categories, including *road*, *sidewalk*, *building*, *wall*, *fence*, *vegetation*, and *terrain etc.* The excellent performance in these classes demonstrates that our model is able to adapt well to the background clutter and pixel distortions introduced by the broader FoV of panoramic images, thus achieving leading segmentation performance.

APPENDIX D MORE QUALITATIVE RESULTS

We showcase more visualization results of panoramic out-of-distribution segmentation of POS on DenseOoS and QuadOoS in Figs. D.1 and D.2. These examples demonstrate that POS achieves excellent performance on the *PanOoS* benchmark. Compared to other mask-transformer-based methods: EAM [23], Mask2Anomaly [25], and RbA [24], POS reduces false positives on the ambiguous background regions and boundaries of inliers while remaining sensitive to outliers. These improvements can be observed more prominently on QuadOoS (see Fig. D.2) under defocus and motion blur scenarios.

APPENDIX E DISCUSSION

E.1 Societal impacts

In this study, we have introduced a novel task called *Panoramic Out-of-distribution Segmentation (PanOoS)* and established a comprehensive benchmark incorporating various well-known baseline models. We found that these baseline models exhibit limited performance on the *PanOoS* task, primarily due to the background clutter and pixel distortions introduced by the panoramic broader FoV. To address this issue, we have developed POS, a solution that significantly enhances the performance of the *PanOoS* benchmark, outperforming existing pinhole-*OoS* methods: pixel-wise architecture and mask-transformer-based method, and achieving promising state-of-the-art results.

PanOoS promotes more comprehensive omnidirectional scene understanding. Our work has the potential to support future

anomaly detection applications for assisting people with visual impairments via robotic guide dogs and wearable robotics. However, it is also possible that it can be applied in the military field, such as for drone omnidirectional perception and autonomous strikes, endangering human safety. In addition, considering that the reliability of deep learning systems for advanced driver assistance systems is crucial, it is important to note that POS may still encounter misclassifications in challenging, intense-motion scenarios, potentially leading to erroneous predictions with adverse societal implications.

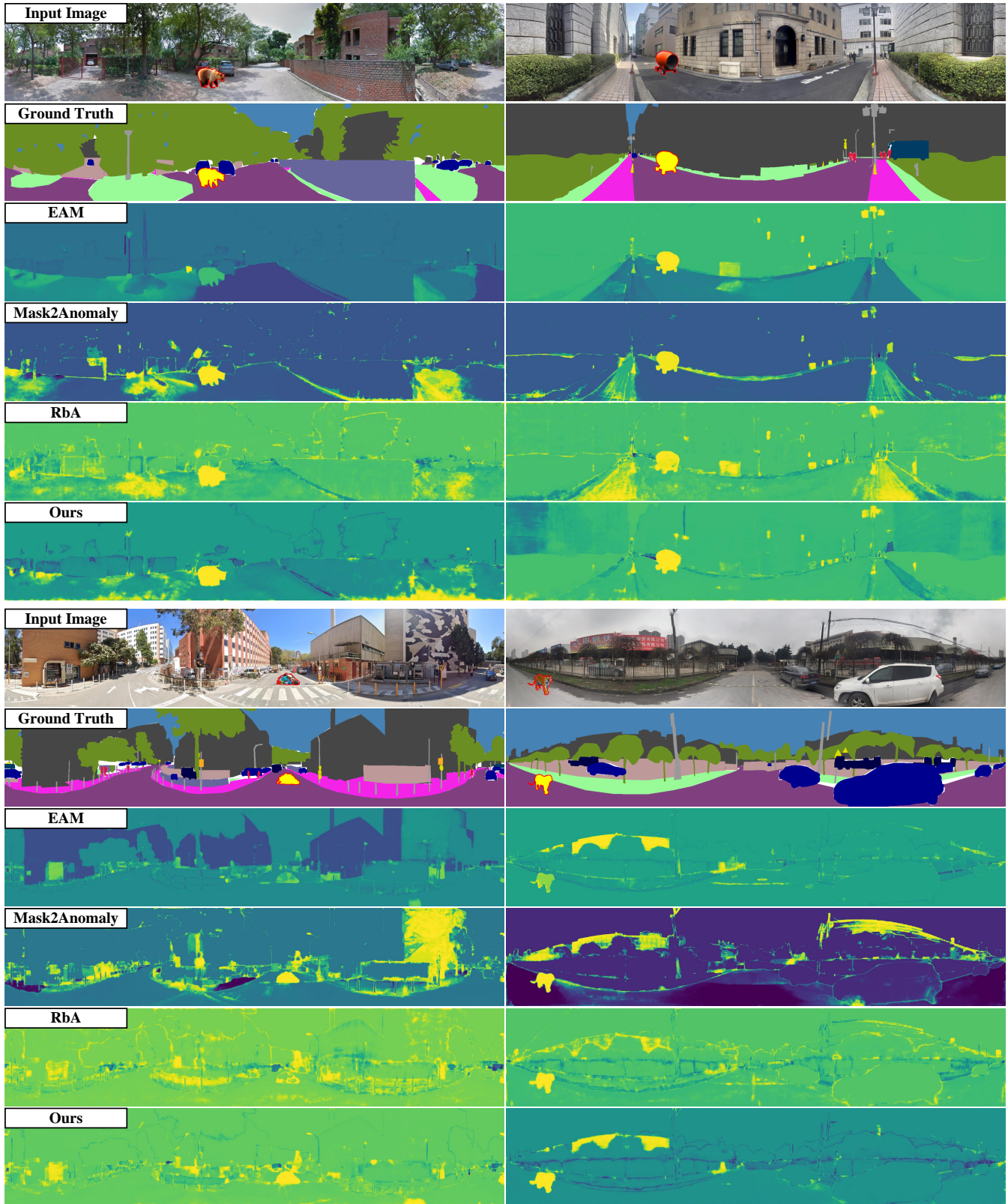


Fig. D.1: Visualization results of *PanOoS* on *DenseOoS*. POS better distinguishes outliers from inliers and produces smoother outlier maps with fewer false positives. Zoom in for a better view.

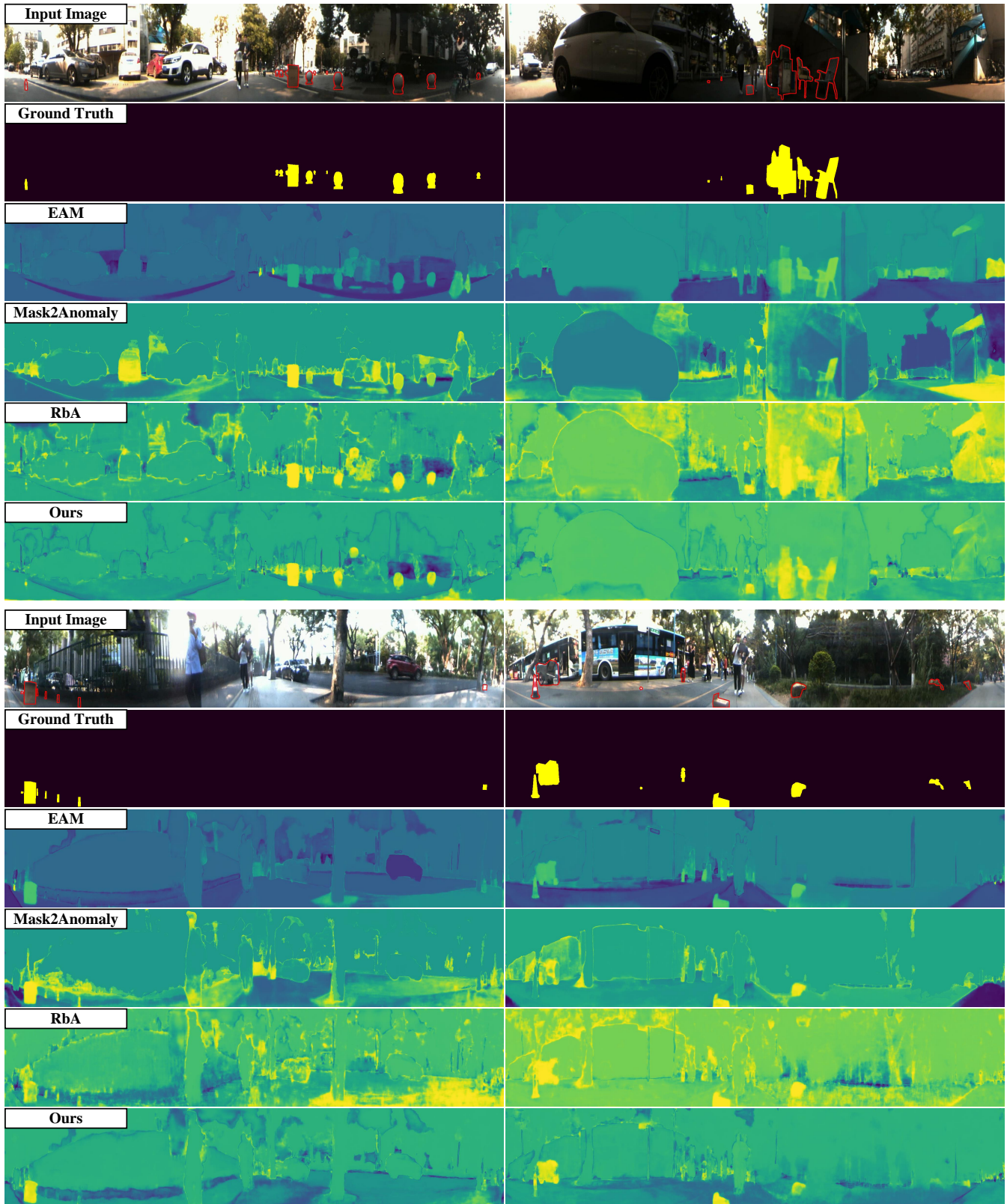


Fig. D.2: **Visualization results of *PanOoS* on *QuadOoS*.** Uneven exposure, defocus, and motion blur caused by dense motion pose extra serious challenges to all methods. The pinhole-*OoS* methods have serious omissions and false positives. However, POS achieves precise segmentation of outliers. Zoom in for a better view.